

DRAFT March 25, 2019

Characterization of M, L and T Dwarfs in the Sloan Digital Sky Survey¹

Suzanne L. Hawley², Kevin R. Covey², Gillian R. Knapp³, David A. Golimowski⁴, Xiaohui Fan⁵,
 Scott F. Anderson², James E. Gunn³, Hugh C. Harris⁶, Željko Ivezić³, Gary M. Long⁴,
 Robert H. Lupton³, Peregrine M. McGehee⁷, Vijay Narayanan³, Eric Peng⁴, David Schlegel³,
 Donald P. Schneider⁸, Emily Y. Spahn⁴, Michael A. Strauss³, Paula Szkody², Zlatan Tsvetanov⁴,
 Lucianne M. Walkowicz⁴, J. Brinkmann⁹, Michael Harvanek⁹, Gregory S. Hennessy¹⁰,
 S. J. Kleinman⁹, Jurek Krzesinski^{9,11}, Dan Long⁹, Eric H. Neilsen¹², Peter R. Newman⁹,
 Atsuko Nitta⁹, Stephanie A. Snedden⁹, Donald G. York¹³

Email: slh@astro.washington.edu, covey@astro.washington.edu, gk@astro.princeton.edu,
 dag@pha.jhu.edu, fan@sns.ias.edu

1. Introduction

Large sky surveys have proven to be fertile ground for identifying extremely late-type stellar and substellar objects (Reid & Hawley 2000). In the past decade, the accumulation of sizable samples of low mass stars and brown dwarfs has been largely the result of near-infrared surveys such as the Deep Near-Infrared Survey (DENIS) (Delfosse et al. 1997) and the Two-Micron All Sky Survey (2MASS) (Skrutskie et al. 1997). These discoveries culminated in the definition of the L spectral class (Kirkpatrick et al. 1999; Martin et al. 1999; Kirkpatrick et al. 2000; Basri et al. 2000).

¹Based on observations obtained with the Sloan Digital Sky Survey and the Apache Point Observatory 3.5-meter telescope, which are owned and operated by the Astrophysical Research Consortium.

²University of Washington, Department of Astronomy, Box 351580, Seattle, WA 98195.

³Princeton University Observatory, Princeton, NJ 08544.

⁴Dept. of Physics and Astronomy, Johns Hopkins University, 3701 University Drive, Baltimore, MD 21218.

⁵The Institute for Advanced Study, Princeton, NJ 08540.

⁶US Naval Observatory, Flagstaff Station, P.O. Box 1149, Flagstaff, AZ 86002.

⁷Los Alamos National Laboratory, MS H820, Los Alamos, NM 87545.

⁸Dept. of Astronomy and Astrophysics, Pennsylvania State University, University Park, PA 16802.

⁹Apache Point Observatory, P.O. Box 59, Sunspot, NM 88349.

¹⁰US Naval Observatory, 3450 Massachusetts Avenue NW, Washington, DC 20392-5420.

¹¹Mt. Suhora Observatory, Cracow Pedagogical University, ul. Podchorazych 2, 30-084 Cracow, Poland.

¹²Fermi National Accelerator Laboratory, P.O. Box 500, Batavia, IL 60510.

¹³University of Chicago, Department of Astronomy and Astrophysics, 5640 S. Ellis Ave., Chicago, IL 60637.

Recently, Sloan Digital Sky Survey (SDSS) photometry was used to identify the first isolated field T dwarfs (Strauss et al. 1999; Tsvetanov et al. 2000) and later to provide candidates that filled the gap separating the L and T spectral sequences (Leggett et al. 2000). Numerous L dwarfs have also been found from SDSS photometry (Fan et al. 2000; Schneider et al. 2002). The reward of these and additional 2MASS efforts has been a well defined spectral sequence from M through T dwarfs (Burgasser et al. 2002; Geballe et al. 2002).

The SDSS offers more than just photometric candidates. The spectral database is expected to ultimately contain more than one million calibrated spectra, many of which will be late type dwarfs. Here we present a study of hundreds of M and L dwarfs compiled from SDSS spectra, together with spectra of SDSS photometric candidates obtained at the 3.5m ARC telescope at Apache Point Observatory (APO). Our final sample also includes all previously published SDSS late-type dwarfs. We first describe the assembly of the sample and the methods used to assign spectral types. We then investigate color–spectral type and color–color relationships, and determine empirical spectroscopic and photometric parallax relations in the red SDSS filters. This paper is intended to provide the necessary calibration information so that SDSS objects may be characterized on the basis of their photometry. Later efforts will be directed at compiling complete samples of objects and using the information described here to determine luminosity and mass functions.

2. Data

Data in our sample include SDSS photometry, 2MASS near-infrared photometry, and spectra obtained from three distinct sources: the SDSS Early Data Release (EDR) (Stoughton et al. 2002), SDSS spectra taken after the EDR, and APO 3.5m telescope followup observations of SDSS photometric candidates. The following sections describe these various data sets.

2.1. SDSS photometry

The SDSS mission is to map a quarter of the sky centered on the North Galactic cap, acquiring accurate photometry of 100 million objects in 5 filters (Fukugita et al. 1996; Gunn et al. 1998) and accumulating over 1 million spectra (York et al. 2000). The survey promises to provide astronomers with an unprecedented source of new astronomical objects. Both photometric and spectroscopic data are obtained with a dedicated 2.5 meter telescope at Apache Point Observatory in New Mexico. The telescope’s 3 degree field is imaged in the 5 filters (u, g, r, i, z) simultaneously by scanning a great circle across the sky at the sidereal rate.¹⁴ Photometric data are automatically reduced by SDSS data processing software (Lupton et al. 2001) and calibrations are obtained from observations with

¹⁴We adopt italics to denote the filters (e.g. u), while asterisks indicate the preliminary calibration of magnitudes within that filter (e.g. u^*).

a 20-inch photometric telescope at the same site (Hogg et al. 2001; Smith et al. 2002). Stoughton et al. (2002) provides information on the central wavelengths and widths of the SDSS filters. See the extensive discussions by Lupton, Gunn & Szalay (1999) and Smith et al. (2002) for further description of the SDSS photometric system. The late type dwarfs reported here are exceedingly red, and many are not detected in the u and g filters. We discuss only r^* , i^* and z^* magnitudes in this paper.

There are two sources of uncertainty in the photometric data that have possible ramifications for late type dwarfs. First, there are slight differences in the response of the detectors used for the z filter observations. Spectral synthesis of L and T dwarfs (Burgasser, private communication) indicates that these differences may introduce z^* magnitude errors of up to 0.1 mags for early L through late T dwarfs. We have not attempted to correct for this source of error. Second, the magnitudes used here are the observed magnitudes, with no correction for reddening. As we show in Section 5.5, some of the early M dwarfs in our sample lie as much as 1.5 kpc distant. We examined the reddening values returned by the SDSS target selection software, which calculates the total Galactic extinction in the SDSS bands using the maps of Schlegel, Finkbeiner & Davis (1998). The reddest objects at each spectral type have typical values $\lesssim 0.1$ in r , $\lesssim 0.07$ in i , and $\lesssim 0.05$ in z . These are upper limits, as most objects are nearby and will have negligible reddening. Therefore, reddening should introduce only a small uncertainty into our photometric parallax relations.

2.2. SDSS spectroscopy

Areas of the sky which have been observed by the SDSS photometric camera provide candidates for spectroscopic observation with the SDSS twin fiber-fed spectrographs. The fibers have 3 arcsec diameter and provide wavelength coverage from 3800Å to 9200Å with resolution $\lambda/\Delta\lambda \sim 1800$. As described by Stoughton et al. (2002), SDSS targets fall into three categories: (1) spectrophotometric and extinction calibration stars and sky fibers; (2) galaxies, luminous red galaxies and quasars, the primary SDSS targets; and (3) additional objects of interest (various categories of stars, objects of unusual color) which use excess fibers in fields of low galaxy density. The last category includes unresolved objects of extremely red color which are late type dwarf candidates. Only objects in categories (1) and (2), plus the very rare brown dwarf candidates, are tiled, i.e. guaranteed a fiber (Stoughton et al. 2002; Blanton et al. 2002), subject to physical limitations which prevent the placement of fibers closer than 55 arcsec apart. During the SDSS commissioning period, the selection criteria for the primary targets were refined and the efficiency improved. Because many of the spectra of late M and L dwarfs are obtained from observations of quasar candidates, especially high-redshift candidates (Richards et al. 2002), the number of such spectra has been declining as the survey progresses, though it is still substantial.

The spectroscopic data are automatically reduced by the SDSS pipeline software which produces spectrophotometrically calibrated spectra including telluric correction. The pipeline also provides spectral classification, emission line identification and redshifts.

2.2.1. Early Data Release spectra

The SDSS EDR contains some 55,000 spectra. Those spectra that met at least one of the following criteria were selected as candidate late type dwarfs: a) colors of $(r^* - i^*) > 1.8$ and $(i^* - z^*) > 1.0$; b) spectrum was identified automatically as a late type star by the SDSS processing software; c) object was targeted for spectral observation as a possible brown or red dwarf on the basis of photometric colors. There is significant overlap between these criteria. The initial sample contained ~ 1000 objects, which was reduced to 626 objects after removing spectra that were too noisy to positively identify with a spectral type, or that were clearly not M, L, or T dwarfs. No additional spectral reduction or calibration was performed aside from rebinning to increase the signal-to-noise ratio.

Using the EDR sample, we investigated the behavior and characteristics of the first implementation of the spectral targetting algorithms. Figure 1 shows the distribution by target category for the M and L dwarfs in our EDR sample. Clearly, most of the objects were targetted as quasars, galaxies or serendipity, the latter because of their unusually red colors. The categories aimed at discovering red and brown dwarfs contributed about 15% of the total, while the other stars and ROSAT selected targets made up the remainder. A large number (120) of the spectra in our sample, nearly all of M dwarfs, were obtained from a single plate of objects targetted to sample the stellar locus and given the arbitrary designation Star: BHB (blue horizontal branch). In general, that category does not contribute a significant number of M and L dwarf targets.

2.2.2. Recent SDSS spectra

An additional sample of candidate late type dwarfs with SDSS spectra (the “recent” sample) was created by searching the SDSS spectral database as of July, 2001 for spectra of objects with $(i^* - z^*) > 1.4$ in order to increase the numbers of very late objects (spectral types M9 and later). This sample, once culled of objects previously identified in the EDR sample, contained about 100 candidates. The number was reduced to 33 after removing extremely noisy spectra and retaining only objects with late M and L spectra. Notably, one previously known T dwarf, SDSSJ1254–0122 was found in this sample. Thus, although the T dwarfs are in general very faint in the SDSS bandpasses, and the SDSS discoveries to date have been confirmed using follow-up observations on other telescopes, a few may emerge with SDSS spectra during the course of the survey.

2.3. APO spectroscopy

Many L and T dwarf candidates identified with SDSS photometry are too faint to be targetted by the SDSS spectrographs, so programs of followup observations on larger telescopes have been initiated. Results from UKIRT, Keck and HET have been previously published (see Section 2.5).

Here we present a collection of 35 previously unpublished spectra obtained with the 3.5m ARC telescope at Apache Point Observatory. Targets were chosen from the photometric database based on their red colors (typically $(i^* - z^*) > 1.6$). The red side of the Double Imaging Spectrograph¹⁵ with the low dispersion grating gave usable wavelength coverage from 6000-10000Å with resolution ~ 600 . Exposure times of 20 minutes at $i^* \sim 19$ and up to an hour at $i^* \sim 20.5$ gave adequate signal-to-noise ratio for spectral typing purposes. For one run, the medium dispersion grating was used, giving resolution ~ 1200 and wavelength coverage 7200-9700Å. Standard data reduction was carried out with IRAF¹⁶ including bias subtraction, flat-field correction, automatic extraction and sky subtraction, and wavelength calibration using exposures of HeNeAr arc lamps. Flux standards (typically O subdwarfs and white dwarfs) were observed each night, and all data were placed on a relative flux scale. On many occasions there were clouds and/or light losses from the (1.5 arcsecond) slit, so the spectra are not uniformly spectrophotometric. We estimate that the relative flux calibration, which is required for our spectral type template fitting procedure (Section 3.3), has a typical uncertainty of 10%. No telluric corrections were applied to the APO spectra.

2.4. 2MASS near-infrared photometry

To supplement the SDSS color information with near-infrared photometry, we searched the public 2MASS database available in December, 2001 for all of our new SDSS objects. Position matches within 2 arcseconds were accepted as detections; more than 95% of the matches were within 1 arcsecond. Approximately 35% of our SDSS sample was detected in 2MASS. This is almost entirely due to the incomplete sky coverage of the public 2MASS data release that is currently available; only four of the M9 and later dwarfs given in Table 5 that are located in the released area were not detected by 2MASS. These four have very faint expected magnitudes, below the 2MASS survey limits. They are noted individually in the table. Thus, when the full 2MASS catalog is made available, we anticipate that most of our objects will have measured near-infrared colors. Unfortunately, none of the objects with spectral types later than L4 and only 6 objects with types L2-L4 were matched, so our near-infrared information is still quite incomplete at the later types. Note that the 2MASS magnitudes are calibrated on a Vega-based magnitude system while the SDSS magnitudes are on the AB _{ν} system (Fukugita et al. 1996).

¹⁵DIS was built by J. Gunn, M. Carr and R. Lupton. A description is available at <http://www.apo.nmsu.edu/Instruments/DIS/dis.html>

¹⁶IRAF is distributed by the National Optical Astronomy Observatories, which are operated by the Association of Universities for Research in Astronomy, Inc., under cooperative agreement with the National Science Foundation.

2.5. Previously published data

We also included data from previously published SDSS late type dwarfs in the sample (Strauss et al. 1999; Fan et al. 2000; Tsvetanov et al. 2000; Leggett et al. 2000; Geballe et al. 2002; Leggett et al. 2002; Schneider et al. 2002). This added 24 objects (14 of the objects with new optical spectra are previously identified SDSS late type dwarfs), many of them late L and T dwarfs that have been confirmed with near-infrared spectroscopy. Three objects were found to have been previously identified by other groups: 2MASSJ1707+6439 (type M9) by Gizis et al. (2000); DENISpJ1159+0057 (type L0) by Martin et al. (1999); and 2MASSWJ0801+4628 by Kirkpatrick et al. (2000).

Some of the published near-infrared photometry was obtained with the Mauna Kea Observatory (MKO) system at UKIRT (Hawarden et al. 2001; Leggett et al. 2002). There are systematic differences between the MKO and 2MASS photometry for these very cool objects. Figure 2 shows the difference in measured J band magnitude as a function of spectral type for 21 objects of type M8 and later which have been measured on both systems (Kirkpatrick et al. 1999, 2000; Burgasser et al. 2002; Leggett et al. 2002). The line is a simple linear fit:

$$J \text{ (2MASS)} - J \text{ (MKO)} = -0.177 + 0.021 \times \text{(spectral type)} \quad (1)$$

applicable between spectral type L0 (10) and T8 (28), with a dispersion of 0.13 mags.¹⁷ We will use the 2MASS J magnitudes extensively in our analysis, so for consistency we convert the published MKO J magnitudes to the 2MASS system using equation 1.

The large dispersion present in the measurements is probably due to the sizable 2MASS uncertainties at these faint magnitudes. One of us (HCH) has independently investigated the J magnitude differences between the two systems. He finds a similar ΔJ relation, indicating that equation 1 is probably more reliable than suggested by the large scatter, at least among the L dwarfs. For the T dwarfs, the data are still too poor to make any firm statement about whether the dispersion is real.

3. Spectral typing

To assign spectral types to the objects in our sample we first compiled a set of high signal-to-noise ratio spectral type standards. We then employed two automatic fitting methods which made use of complementary information. In the first method, spectral indices of individual features

¹⁷The numerical spectral type in equation 1 follows standard convention and is used throughout this paper: M0=0, M5=5, L0=10, L5=15, T0=20, and so forth through T8=28.

were measured and compared to a standard sequence, following Reid, Hawley & Gizis (1995) and Kirkpatrick et al. (1999) (hereafter K99). The second method used a least squares fitting algorithm to match primarily the continuum shape to the spectral type standards, as described by Kirkpatrick et al. (1991) and Henry et al. (2002). The two methods provided independent measures of the spectral type. Each spectrum was then examined visually by two of us (SLH, KRC) and a final type assigned.

3.1. Standards

The spectral type standards used as templates in the least squares fitting routine are listed in Table 1. The late M and L dwarfs were chosen from the standards described in K99 and Kirkpatrick et al. (2000) (hereafter K00), and used to define their L dwarf sequence. The early-mid M dwarfs were chosen from the list of primary spectral type standards used to define the M dwarf sequence by Kirkpatrick et al. (1991) (except GJ1141B which was taken from Reid, Hawley & Gizis (1995)). The APO 3.5m data in Table 1 were obtained by us for this purpose, and have the same resolution and wavelength coverage as the majority of the data described in Section 2.3. The Keck data have been made public courtesy of Neill Reid¹⁸ and are described in K99 and Kirkpatrick et al. (2000).

3.2. Spectral indices method

The standards listed in Table 1, and a number of additional objects with well-known spectral types from the same references, were measured to develop polynomial relationships between spectral type and individual spectral features. We first implemented the spectral indices suggested in K99 for the L dwarf sequence, which combine measurements of molecular bands (CrH, TiO, VO) and atomic lines (Rb I, Cs I) as described therein. Specifically, we computed their indices CrH-a, Rb-b/TiO-b, Cs-a/VO-b and Color-d. Our task was immediately complicated by two problems: our spectra have lower resolution and generally lower signal-to-noise ratio compared to the Keck spectra used by K99. Thus, for example, our Rb I and Cs I line measurements were usually too noisy to give useful results. We therefore tried numerous additional diagnostics, settling finally on the set described in Table 2. In the early-mid M dwarf range, we also computed the TiO5 and CaH3 indices, which are defined and used extensively for spectral typing in the PMSU survey of 2000 M dwarfs in the Solar Neighborhood (Reid, Hawley & Gizis 1995; Hawley, Gizis & Reid 1996).

Figure 3 shows most of the new indices defined here, together with the TiO5 and CaH3 indices for reference. Open triangles indicate stars with spectral types M0-M8, while the pluses are M9-L8 dwarfs. All of the indices reverse strength near spectral type M8, necessitating two part fits as shown with dotted and solid lines for the earlier and later types, respectively. VO7912 reverses

¹⁸See the website at www.physics.upenn.edu/~inr for links to these data.

strength again near type L4 (similar to the behavior of CrH-a in the K99 scheme) so we did not use it for fitting the later type dwarfs. VO7434 was also useful only to type L6. Color-d as defined in K99 provides useful information, but it includes measurements at red wavelengths that are not observed in the SDSS spectra. Therefore we tried our index Color-1 (not shown in the figure), but it provided only limited information on the mid-late L dwarfs and was not useful for earlier type dwarfs. Figure 3 highlights the particular difficulty with classifying objects in the M7-L1 range as nearly all of the indices overlap in this spectral type region. We relied more heavily on the template fitting results and examination by eye for those objects.

The final type produced by the spectral indices method consisted of an average of the types given by each individual index. The M and L types were computed separately for each object using the M and L fits to the indices, respectively. The standard deviation of the average type usually gave a good indication of which type (M or L) was more appropriate. However, inspection by eye and comparison with the template type was required to ensure that the automatic indices type was reasonable.

3.3. Template fitting method

Our template fitting method followed closely the procedure outlined by Henry et al. (2002) (hereafter H02), using a modified version of their ALLSTAR program. The SDSS candidate spectrum was interpolated onto a 1Å wavelength scale, smoothed with a 25Å window function, and normalized to the flux in the region 8651-8661Å. This differs slightly from the H02 procedure; they do not smooth their spectra, which typically have much higher signal-to-noise ratio, and they normalize their spectra at 7500Å. We required a location where there was more flux and hence a better signal-to-noise ratio in the very cool late M and L dwarfs, and which avoided the broad blue wing of the K I feature. As described by H02, to compensate for anomalous errors caused by noise in the normalization region, the candidate spectrum was multiplied by a factor from 0.9 to 1.1 in steps of 0.01. The template spectra (also normalized to the 8651-8661Å region) were then successively fit by least squares to the 21 scaled candidate spectra, and the best match (lowest sum of mean squared residuals) for each template was recorded. Deviant pixels were treated with 2σ rejection as in the H02 description. When all templates (M0-L8) had been fit, the 3 best fits were reported. We had additional confidence in the fit if the 3 best matches gave both low residuals and neighboring spectral types.

Before being implemented on the SDSS sample, the algorithm was first tested by adding Gaussian noise to spectra of objects with known spectral types to achieve signal-to-noise ratios ranging from 2 to 40 (per Å), and optimizing parameters (smoothing width, normalization location, etc.) such that the objects were re-identified as correctly as possible, resulting in the parameters described above. Our results from testing both the indices and template methods on spectra of objects with known types (but not the templates themselves when testing the template method!) are shown in Figure 4. The good agreement indicates that the methods are independently reliable,

and each is able to predict the spectral type within ~ 1 spectral class for both M and L dwarfs.

Finally, we note that the template method presumes accurate relative flux calibration for both template and program data. Both the APO and Keck data, as well as the SDSS data, proved to have adequate relative spectrophotometry as shown by the good agreement between the template and indices typing methods for nearly all objects.

3.4. Final Types

After being typed automatically by both the indices and template methods, the spectra were examined by eye. If the two measures gave different results, a final type was assigned by visual inspection and comparison to templates. There are two previously known T dwarfs for which we have new optical spectra. We classified these as T:: by visual inspection, as the spectra appeared to be later than our latest L dwarf template. Ultimately, 616 M dwarfs, 42 L dwarfs, and 1 T dwarf were typed on the basis of their SDSS spectra, and an additional 13 Ms, 21 Ls, and 1 T were typed using APO spectra.

We estimate that this complete method of spectral typing gives types with an uncertainty of ± 1 spectral type for the M and L dwarfs presented here. This uncertainty estimate is bolstered by considering that 1) objects with multiple spectra were consistently typed with identical or neighboring spectral types; and 2) our spectral types match those of other groups within ~ 1 spectral type for the few stars in common (see Table 5).

4. Results

The large number of early and mid M dwarfs prohibits showing individual spectra of all objects. Instead, we provide the mean and standard deviation for several optical and near-infrared colors at each spectral type in Table 4.¹⁹ Our highest signal-to-noise ratio SDSS spectrum for each spectral type (M0-L4) is shown in Figure 5(a,b). The signal-to-noise ratios range from 10 (at type L4) to 50 (at type M3), measured at our normalization region near 8650Å. This set of SDSS standard spectra has been submitted to the collaboration for inclusion in the spectral pipeline software to assist in assigning automatic types to late type dwarfs during the SDSS processing.²⁰

Individual photometric and spectral type information for all dwarfs with types M9 and later are given in Table 5. Near-infrared data are from 2MASS except where noted, and the K magnitudes are therefore measured in the K_s filter (see K99 for discussion of this filter bandpass and typical

¹⁹We will make available the data file giving individual information for each star upon request. Contact the first author at the email address given.

²⁰These spectra are also available upon request.

effects in late type dwarfs). The M9 and L dwarf spectral types are ours, with the exception of SDSSJ0830+4828 which has a previously determined type of L9 based on its near-infrared spectrum (Geballe et al. 2002). All objects with previously determined spectral types are noted, and the references are given in the table notes. For the late L dwarfs, differences between optical and near-infrared spectral types have been discussed by Geballe et al. (2002). However, the few objects in common in our sample do not appear to differ systematically in type. All T dwarfs have spectral types determined from near-infrared spectra.

Typical photometric errors for the r^* data in Table 5 are (in magnitudes): $\lesssim 0.02$ for $r^* < 20$; 0.05 at $r^* = 21$; 0.1 at $r^* = 22$; 0.25 at $r^* = 23$; and 0.5 at $r^* = 24$. As described by York et al. (2000) and the table notes, the nominal 5σ detection limit is $r^* = 23.1$. We have indicated detections fainter than this limit with an asterisk, and individual measurements with uncertainty greater than 0.5 magnitudes with a colon.

The i^* and z^* photometry are brighter for these very red objects. Photometric errors in i^* range from $\lesssim 0.05$ for $i^* < 20$ to 0.2 at $i^* = 22.5$; corresponding values for z^* are $\lesssim 0.05$ for $z^* < 19$ and 0.2 at $z^* = 21$. The nominal 5σ detection limits are $i^* = 22.3$ and $z^* = 20.8$. Again we indicate detections fainter than these limits with an asterisk, and note uncertainties greater than 0.2 magnitudes in the i^* and z^* measurements with a colon.

Spectra for the M9 and later objects are shown in Figure 6(a-f) for the SDSS spectra and Figure 7(a-d) for the APO spectra. The SDSS spectra have been smoothed by 11 pixels and the APO spectra have been smoothed by 3 pixels. The smoothing amounts to $\sim 20\text{\AA}$ in each case. The signal-to-noise (S/N) ratios range from 2-10 for these spectra, measured at the normalization region near 8650\AA . For reference, the M9 dwarf SDSSJ0249-0034 (Figure 6a) has a relatively high S/N ratio ~ 10 ; the M9 dwarf SDSSJ1719+6053 (Figure 6b) has moderate S/N ratio ~ 5 ; and the L6 dwarf SDSSJ0236+0048 (Figure 6f) has low S/N ratio ~ 2 .

5. Discussion

The total sample assembled for this paper, including our new identifications and those previously published, consists of 718 SDSS late type dwarfs (632 M, 76 L, and 10 T). All have well-determined spectral types and photometric measurements in i^* and z^* . Many also have r^* and/or near-infrared data. This sample allows us to investigate the color–spectral type and color–color relationships in the SDSS and near-infrared colors. Using a calibrated spectral type – absolute J magnitude relation for objects with known distances, we can determine absolute magnitude relations in the SDSS filters. Finally, we use those relations to estimate distances for the sample. We caution that the present sample is not complete within either distance or apparent magnitude limits, as the selection of spectra from the various SDSS targetting algorithms gives neither homogeneous nor fully sampled results. The sample as it stands is therefore not useful for luminosity or mass function determinations. Rather, we seek to provide the necessary color, spectral type and

absolute magnitude calibration information to be used in a future study, when complete samples are available.

5.1. Color – spectral type relations

Figure 8 shows the correlation between color and spectral type for six different colors: two optical SDSS colors $[(r^* - i^*), (i^* - z^*)]$, three optical–near-infrared colors $[(i^* - J), (z^* - J), (z^* - K)]$, and one near-infrared color $[(J - K)]$. We do not present any results for colors using H magnitudes as they are very similar to the results for colors formed with K magnitudes and do not provide additional useful diagnostics. Note again that the objects with MKO J-band magnitudes have been converted via equation 1 to the 2MASS J-band system. No correction was attempted for the MKO K-band magnitudes so colors that include K photometry may have systematic offsets for those objects. We have not used colors that include the K-band in any of our numerical fitting.

The SDSS $(r^* - i^*)$ color peaks at ~ 2.8 near spectral type M8. Later type objects apparently become somewhat bluer, with late L dwarfs having similar $(r^* - i^*)$ colors to mid M dwarfs. However, the r^* photometry is very uncertain for the later objects, and it may be that $(r^* - i^*)$ simply flattens at ~ 2 with large observational scatter for dwarfs of mid L and later types. The $(r^* - i^*)$ color by itself is not a good diagnostic for dwarfs later than type M8.

The $(i^* - z^*)$ color does not show such a turnover; it increases monotonically from early M into the T dwarfs. However, it is quite flat at ~ 1.8 between M9–L3 (see also Schneider et al. (2002)), and appears to flatten in the T’s at ~ 4.0 though with large scatter (probably due to uncertainty in the i^* measurements at these faint magnitudes). It is very useful for identifying candidate late type dwarfs: $(i^* - z^*) > 1.6$ will pick out objects M8 and later (as noted by Strauss et al. (1999) who found the first isolated T dwarf using its very red $(i^* - z^*)$ color). If one has only optical (SDSS) colors, it is possible to partially discriminate for very late objects by first requiring $(i^* - z^*) > 1.6$, and then choosing objects with bluer $(r^* - i^*)$ colors (e.g. $\lesssim 2.0$). A problem with this approach is that those objects are very faint, and often do not have good r^* photometry, so the $(r^* - i^*)$ colors may not be reliable.

The $(I - J)$ color, where I is the Cousins I band, was shown by Reid et al. (2001) to be a good spectral type discriminant from M through T. Here we plot $(i^* - J)$, which shows similar behavior to $(i^* - z^*)$, but with the flattening confined to types L2–L4 at $(i^* - J) \sim 4.7$, and the T dwarfs all having $(i^* - J) \sim 7$. An advantage of $(i^* - J)$ is that it covers a large total range in color, varying from $2 < (i^* - J) < 8$ between early M and late T.

The $(z^* - J)$ color is rather flat, with large scatter, through the mid-L range (L2–L7). It is not clear if this scatter represents intrinsic variations in the objects, or if it is just the result of small numbers and uncertain data. The $(z^* - J)$ color does change systematically through the late-M and early-L regime, where the spectral types are not easy to distinguish spectroscopically (see Section 3.2). Interestingly, the $(z^* - J)$ color shown here behaves somewhat differently than the

(Z-J) color discussed by Leggett et al. (2002), which uses the MKO Z and J filters. Their (Z-J) color is flat at ~ 1.7 between mid-L and mid-T types. Presumably this is related to differences in the filter bandpasses and detector sensitivities.

The ($z^* - K$) color is very well behaved from M through mid L types, showing a monotonic increase with little scatter. However, it turns over and becomes blue in the late L and T dwarfs where methane absorption dominates the K band.

Finally, the (J-K) color has been investigated previously for late type dwarfs (Reid 1993; Kirkpatrick et al. 1999; Leggett et al. 2002). As discussed by those authors, it is of limited usefulness, showing small range in the M dwarfs and large scatter among the L dwarfs. It also becomes blue in the T dwarfs, again because of methane absorption in the K band.

In summary, ($i^* - z^*$) and ($i^* - J$) provide spectral type information across most of the range from M through T. The ($z^* - J$) and ($z^* - K$) are useful discriminators in the spectral type ranges where ($i^* - z^*$) and ($i^* - J$) flatten. A combination of optical and near-infrared photometry allows a reasonable determination of the spectral type at least through the M and L dwarf classes. The sparse and relatively uncertain data on T dwarfs make the color-spectral type relations still poorly defined for those objects.

5.2. Color – color relations

Figure 9 shows several color-color relations for the sample. The spectral type of each object is coded by symbol, given in the figure caption, to verify that indeed the color-color relations are mapping the spectral sequence. As expected from the behavior of ($r^* - i^*$) and ($i^* - z^*$) described above, the ($r^* - i^*$) vs ($i^* - z^*$) diagram is not useful past the mid-M dwarfs, with objects M5-L4 occupying the same region of color–color space. The ($r^* - i^*$) vs ($i^* - J$) diagram is somewhat more spread out, but still shows significant overlap in spectral type at the same colors. Both the ($i^* - z^*, z^* - J$) and the ($i^* - J, z^* - J$) diagrams show significant overlap in the L dwarfs, with the latter providing a better sequence from M through early L. The ($z^* - J, z^* - K$) diagram is also well-behaved in the M and early L regimes, but has significant overlap between mid and late L dwarfs and turns over in the T dwarfs where the K band flux is diminished by methane absorption. Overall, the color–color plot which provides the best spectral type discrimination is ($i^* - z^*, i^* - J$) which shows only a mild flattening in the early L’s, but otherwise provides a monotonic sequence from early M through late T. The average colors at each spectral type given in Table 4 provide the information necessary to assign a spectral type if optical and near-infrared photometry are available.

5.3. Spectroscopic parallaxes

Our ultimate goal is to determine photometric relations between color, spectral type and absolute magnitude that will allow us to find the spectral type and distance of an object without needing to take a spectrum. The previous sections describe the color-spectral type relations, and we now investigate parallax relations. Unfortunately the sample of objects with both measured trigonometric parallax and measured SDSS colors is much too small at present to provide a useful calibration. Instead, we must employ a two-step process where we first use a well-observed sample of nearby MLT dwarfs with measured trigonometric parallaxes, 2MASS J magnitudes and spectral types to calibrate a spectroscopic parallax relation. We then apply this relation to our SDSS sample and obtain parallax estimates which we combine with the SDSS colors to get photometric parallax relations. Eventually, as more trigonometric parallaxes are obtained for SDSS targets, we expect that the SDSS photometric parallax relation will be calibrated directly and it will not be necessary to resort to a spectroscopic parallax relation for calibration.

Figure 10 shows our M_J spectroscopic parallax relation, incorporating the eight parsec sample distances (Reid & Gizis 1997; Reid & Hawley 2000) for types M0-M7, and distances quoted by Leggett et al. (2002) (see references therein) for objects with types M8 and later. New distances from Dahn et al. (2002) were available for five objects (DENISpJ0205-1159, 2MASSJ0559-1404, 2MASSJ0850+1057, SDSSJ1254-0122, SDSSJ1624+0029). We applied the magnitude differences for the resolved L dwarf binaries described by Reid et al. (2001) to correct the absolute magnitudes for those objects. Only objects with measured 2MASS J magnitudes are included (i.e. those objects that were only measured in other systems were left out rather than being transformed to the 2MASS system).

The early M dwarfs show the well-documented drop in luminosity near spectral type M4 (Hawley, Gizis & Reid 1996; Reid & Gizis 1997), making fitting difficult. It appears that there is also a change in slope near spectral type M8, and another drop in luminosity near type L6. The latter effect is poorly defined, and clearly more parallaxes of objects near this type are required. In addition, spectral types for the late L and T dwarfs are based on near-infrared spectra, while those for the M and early-mid L dwarfs are based on optical spectra. This may introduce systematic effects which could contribute to the apparent discontinuity at L6. We therefore caution that the relation for the L6-T8 dwarfs remains ill-defined at present.

Numerous instances of incorrect fitting which propagated into incorrect luminosity and mass function determinations exist in the literature (see (Reid & Hawley 2000)). Therefore, we chose to be very conservative in our fit to the M_J – spectral type relation shown here. We adopt a fit consisting of several line segments, together with a single value for type M4. Our best fit relations are given by:

$$\begin{aligned}
 M_J &= 6.46 + 0.26 \times (\text{spectral type}) & (K7-M3) \\
 M_J &= 8.34 & (M4) \\
 M_J &= 5.73 + 0.74 \times (\text{spectral type}) & (M5-M7) \\
 M_J &= 8.83 + 0.29 \times (\text{spectral type}) & (M8-L5) \\
 M_J &= 12.13 + 0.14 \times (\text{spectral type}) & (L6-T8)
 \end{aligned} \tag{2}$$

Note that all T dwarfs with known distances are shown, but 2MASSJ0559-1404 (T4) and Gl 229B (T6), indicated by open triangles in the figure, are not included in the fit. The former is omitted because it lies several magnitudes above the best fit line and has an undue influence on it. Burgasser (2001) discusses this T4 dwarf in detail, and notes that it has an unusual flux distribution which may indicate it is a binary system. Gl 229B has a UKIRT J magnitude and we chose to use only those objects with 2MASS J magnitudes. In any case, it does not significantly alter the fit.

Figure 10 allows us to assign M_J values to the objects with measured J magnitudes in our sample. With our measured colors, we may then compute M_{r^*} , M_{i^*} and M_{z^*} spectroscopic parallax relations as shown in Figure 11. The M_{z^*} relation retains some signature of the discontinuity near L6, but all three relations are fairly well-behaved. Absolute magnitudes may thus be assigned in any of the red SDSS filters if the spectral type is known. We have not attempted to fit the other absolute magnitude - spectral type relations, but Table 4 includes the M_J values together with the average colors, so the average absolute magnitude in r^*, i^* and z^* may easily be computed at each spectral type.

5.4. Photometric parallaxes

Using the spectroscopic parallax results from the previous section, we can now investigate photometric parallax relations. Figure 12 shows the results for the colors $(r^* - i^*)$, $(i^* - z^*)$, $(i^* - J)$ and $(z^* - J)$. We did not compute relations using colors involving the K band, because those colors turn over and become bluer in the T dwarfs. The $(r^* - i^*)$ color is not useful, as expected from its behavior in Figure 8. The $(z^* - J)$ plots show the effect of the discontinuity at L6 quite strongly, with significant color overlap between early and late L dwarfs. Not surprisingly, the best relations are those using the $(i^* - z^*)$ and $(i^* - J)$ colors. Figure 13 shows the two relations for which reasonable least squares fits were obtained with second order polynomials to the average colors from Table 4. The fits are:

$$M_{i^*} = 4.471 + 7.907(i^* - z^*) - 0.837(i^* - z^*)^2$$

$$M_{i^*} = 1.213 + 4.379(i^* - J) - 0.195(i^* - J)^2 \quad (3)$$

The second fit (M_{i^*} , $i^* - J$) has slight systematic residuals at the discontinuities near M4 ($i^* - J \sim 3$) and L6 ($i^* - J \sim 5$), and should be used with caution.

5.5. Distance distribution

The approximate distance limits to which the SDSS is probing the late type dwarf population can be estimated using these parallax relations. Figure 14 is a plot of log distance vs spectral type for all of the sample objects. The distances were obtained from the mean spectral type - absolute magnitude relations given in Table 4. Distances obtained from the photometric parallax relations in equation 3 typically agree within 25%, and the photometric distance estimates are unbiased when compared to those found from the spectroscopic parallax relations (i.e. the mean distance differences for the sample are close to zero).

It appears that early M dwarfs are present in the sample out to almost 1.5 kpc, but the distance limit rapidly decreases at later types. The SDSS imaging has bright magnitude limits of ~ 14 in r^* and i^* and ~ 12 in z^* , while spectroscopic targetting is limited to objects fainter than $r^* \sim 15$ to minimize scattered light in the spectra (Stoughton et al. 2002). This explains the lack of nearby early-mid M dwarfs in the sample. L dwarfs are being observed to ~ 100 pc, which is not unexpected given the magnitude limits ($i^* \sim 19-21$) of the various targetting algorithms and the monotonic decrease in luminosity for objects of later types. The T dwarf results imply a distance limit of ~ 20 pc, but the distance estimates are less reliable considering the large scatter in the calibrated M_J – spectral type relation (Figure 10), the statistical correction which had to be applied to the measured MKO J magnitudes for several of the objects, and the sparse sample. The two SDSS T dwarfs with trigonometric parallax measurements (SDSSJ1254-0122, 11.8 pc; SDSSJ1624+0029, 10.9 pc; Dahn et al. (2002)) have predicted distances of 8.9 pc and 8.1 pc respectively.

6. Summary

We have compiled a large sample of M, L and T dwarfs discovered in the Sloan Digital Sky Survey imaging data. New objects have followup SDSS or APO optical spectroscopy. About 35% of the sample also has near-infrared photometry. In combination with previously published SDSS objects, a final sample of 718 objects was analyzed. Color–spectral type and color–color relations for several optical and near-infrared colors were examined, and the $(i^* - z^*)$ and $(i^* - J)$ colors were found to be the most useful for estimating spectral types based solely on photometric information.

We then employed a spectroscopic parallax relation for nearby dwarfs with known distances to investigate spectroscopic and photometric parallaxes in the SDSS filters. The $(i^* - z^*)$ and $(i^* - J)$

colors gave good estimates of M_{i*} and hence are useful distance indicators. Our distance estimates show that SDSS is finding early M dwarfs at distances > 1 kpc, L dwarfs to distances ~ 100 pc, and T dwarfs out to 20 pc. Thus, the SDSS will provide numerous examples of the latest type dwarfs, and the early M dwarfs should be useful for probing Galactic structure. The next step is to compile samples that are complete to some distance and/or apparent magnitude limit, in order to investigate the luminosity and mass functions of these late type dwarfs. Additional efforts will be aimed at investigating the magnetic activity properties of the sample, the incidence of subdwarfs, and possible photometric metallicity indicators.

The Sloan Digital Sky Survey (SDSS) is a joint project of The University of Chicago, Fermilab, the Institute for Advanced Study, the Japan Participation Group, The Johns Hopkins University, the Max-Planck-Institute for Astronomy (MPIA), the Max-Planck-Institute for Astrophysics (MPA), New Mexico State University, Princeton University, the United States Naval Observatory, and the University of Washington. Apache Point Observatory, site of the SDSS telescopes and the 3.5-meter telescope, is operated by the Astrophysical Research Consortium (ARC).

Funding for the project has been provided by the Alfred P. Sloan Foundation, the SDSS member institutions, the National Aeronautics and Space Administration, the National Science Foundation, the U.S. Department of Energy, the Japanese Monbukagakusho, and the Max Planck Society. The SDSS Web site is <http://www.sdss.org/>.

We acknowledge generous support from Princeton University and NASA via grant NAG5-6734.

This research has made use of NASA's Astrophysics Data System Abstract Service, the SIMBAD database, operated at CDS, Strasbourg, France, and the Two Micron All Sky Survey (2MASS) Second Incremental Release Point Source Catalog (PSC), a joint project of the University of Massachusetts and the Infrared Processing and Analysis Center/California Institute of Technology, funded by the National Aeronautics and Space Administration and the National Science Foundation.

REFERENCES

Basri, G. et al. 2000, *ApJ*, 538, 363

Blanton, M.R. et al. 2002, *AJ*, in press

Burgasser, A. J., Kirkpatrick, J. D., Brown, M. E., Reid, I. N., Gizis, J. E., Dahn, C. C., Monet, D. G., Beichman, C. A., Liebert, J., Cutri, R. M.; Skrutskie, M. F. 1999, *ApJ*, 522, L65

Burgasser, A.J. 2001, *ASP Conf. Ser.* 231, 477 (ed. C.E. Woodward, M.D. Bicay, J.M. Shull)

Burgasser, A.J., et al. 2002, *ApJ*, 564, 421

Dahn, C.C. et al. 2002, *AJ*, submitted

Delfosse, X., Tinney, C. G., Foreville, T., Epchtein, N., Bertin, E., Borsenberger, J., Copet, E., De Batz, B., Fouque, P., Kimeswenger, S., Le Bertre, T., Lacombe, F., Rouan, D., Tiphene, D. 1997, *A&A*, 327, L25

Fan, X., et al. 2000, *AJ*, 119, 928

Fukugita, M., Ichikawa, T., Gunn, J. E., Doi, M., Shimasaku, K., Schneider, D. P. 1996, *AJ*, 111, 1748

Geballe, T. R., et al. 2002, *ApJ*, 564, 466

Gizis, J.E. et al. 2000, *AJ*, 120, 285

Gunn, J.E., Carr, M.A., Rockosi, C.M., Sekiguchi, M., et al. 1998, *AJ*, 116, 3040

Hawarden, T.G., Leggett, S.K., Letawsky, M.B., Ballantyne, D.R., Casali, M.M. 2001, *MNRAS*, 325, 563

Hawley, S.L., Gizis, J.E., & Reid, I.N. 1996, *AJ*, 112, 2799

Henry, T.J., Walkowicz, L.M., Barto, T.C., Goliowski, D.A. 2002, *AJ*, in press (H02)

Hogg, D. W., Finkbeiner, D.P., Schlegel, D.J., Gunn, J.E. 2001, *AJ*, 122, 2129

Kirkpatrick, J.D., Henry, T. J., McCarthy, D. W., Jr. 1991, *ApJS*, 77, 417

Kirkpatrick, J.D., Reid, I. R., Liebert, J., Cutri, R. M., Nelson, B., Beichman, C. A., Dahn, C. C., Monet, D. A., Gizis, J. E., Skrutskie, M. F. 1999, *ApJ*, 519, 802 (K99)

Kirkpatrick, J.D., Reid, I. R., Liebert, J., Gizis, J. E., Burgasser, A. J., Monet, D. A., Dahn, C. C. 2000, *AJ*, 120, 447

Leggett, S. K., et al. 2000, *ApJ*, 536, L35

Leggett, S. K., et al. 2002, *ApJ*, 564, 452

Lupton, R.H., Gunn, J.E. & Szalay, A.S. 1999, *AJ*, 118, 1406

Lupton, R. H., Gunn, J. E., Ivezić, Ž., Knapp, G. R., Kent, S. M., Yasuda, N. 2001, in *Proceedings of ADASS X*, ed. F.R. Harnden Jr., F.A. Primini and H. E. Payne, *ASP Conf. Ser.* 238, 269

Martin, E. et al. 1999, *AJ*, 118, 2466

Reid, I.N. 1993, *Ap&SS*, 217, 57

Reid, I.N., Hawley, S.L., & Gizis, J.E. 1995, *AJ*, 110, 1838

Reid, I.N., & Gizis, J.E. 1997, *AJ*, 113, 2246

Reid, I.N., Kirkpatrick, J.D., Liebert, J., Burrows, A., Gizis, J.E., Burgasser, A., Dahn, C.C., Monet, D., Cutri, R., Beichman, C.A., & Skrutskie, M 1999, *ApJ*, 521, 613

Reid, I.N., & Hawley, S.L. 2000, *New Light on Dark Stars: Red Dwarfs, Low-Mass Stars, and Brown Dwarfs* (New York, Springer-Praxis)

Reid, I.N., Gizis, J.E., Kirkpatrick, J.D. & Koerner, D.W. 2001, *AJ*, 121, 489

Richards, G.T. et al. 2002, *AJ*, submitted

Schneider, D. P., et al. 2002, *AJ*, in press, astro-ph 0110273

Schlegel, D.J., Finkbeiner, D.P., Davis, M. 1998, *ApJ*, 500, 525

Skrutskie, M. F., et al. 1997, in *The Impact of Large-Scale Near-IR Sky Surveys*, ed. F. Garzon et al. (Dordrecht: Kluwer), 25

Stoughton, C., et al. 2002, *AJ*, in press

Strauss, M. A., et al. 1999, *ApJ*, 552, L61

Smith, J.A. et al. 2002, *AJ*, in press, astro-ph 0201143

Tsvetanov, Z. I., et al. 2000, *ApJ*, 531, L61

York, D. G., et al. 2000, *AJ*, 120, 1579

Table 1. Template Information

Spectral Type	Object Name	Observatory
M0	Gliese 270	APO
M1	GJ 1141B	APO
M2	Gliese 220	APO
M3	Gliese 251	APO
M4	Gliese 213	APO
M5	Gliese 51	APO
M6	2MASS 0435+1537	KECK
M7	2MASS 0055+2756	KECK
M8	2MASS 1047+4026	KECK
M9	2MASS 0251+2521	KECK
L0	2MASS 0345+2540	KECK
L1	2MASS 1439+1929	KECK
L2	Kelu-1	KECK
L3	DENIS 1058–1548	KECK
L4	2MASS 1506+1321	KECK
L5	2MASS 1507–1627	KECK
L6	2MASS 0103+1935	KECK
L7	DENIS 0205–1159	KECK
L8	2MASS 1632+1904	KECK

Table 2. Spectral Type Indices for SDSS M and L Dwarfs

index name	numerator Å	denominator Å
VO 7434	7430-7470	7550-7570
VO 7912	7900-7980	8400-8420
Na 8190	8140-8165	8173-8210
TiO 8440	8440-8470	8400-8420
Color-1	8900-9100	7350-7550

Note. — The weighted (by the variance) average of the flux density F_λ in the numerator and denominator wavelength regions are each computed. The index consists of the ratio with its associated uncertainty.

Table 4. Average Color by Spectral Type

Spectral Type	$r^* - i^*$	$i^* - z^*$	$z^* - J$	$i^* - J$	M_J
M0	0.91 (0.24)	0.49 (0.06)	1.42 (0.50)	1.93 (0.50)	6.45
M1	0.99 (0.28)	0.50 (0.29)	1.25 (0.08)	1.78 (0.10)	6.72
M2	1.09 (0.26)	0.62 (0.17)	1.36 (0.18)	1.94 (0.20)	6.98
M3	1.29 (0.32)	0.73 (0.24)	1.38 (0.12)	2.08 (0.13)	7.24
M4	1.57 (0.33)	0.87 (0.32)	1.52 (0.13)	2.39 (0.17)	8.34
M5	1.98 (0.25)	1.09 (0.13)	1.65 (0.09)	2.72 (0.13)	9.44
M6	2.27 (0.19)	1.27 (0.14)	1.74 (0.08)	2.99 (0.19)	10.18
M7	2.67 (0.22)	1.52 (0.11)	1.95 (0.16)	3.47 (0.24)	10.92
M8	2.82 (0.28)	1.62 (0.11)	2.04 (0.12)	3.72 (0.19)	11.14
M9	2.89 (0.44)	1.79 (0.20)	2.23 (0.14)	4.09 (0.28)	11.43
L0	2.64 (0.25)	1.85 (0.11)	2.36 (0.14)	4.23 (0.19)	11.72
L1	2.56 (0.27)	1.92 (0.08)	2.52 (0.08)	4.45 (0.08)	12.00
L2	2.50 (0.47)	1.85 (0.09)	2.76 (0.36)	4.64 (0.45)	12.29
L3	2.34 (0.39)	2.00 (0.24)	2.71 (0.19)	4.84 (0.50)	12.58
L4	2.38 (0.27)	2.26 (0.13)	2.80 (0.08)	5.06 (0.18)	12.87
L5	2.00 (0.40)	2.47 (0.12)	2.74 (0.23)	5.21 (0.32)	13.16
L6	2.79 (0.69)	2.40 (0.19)	2.86 (0.15)	5.27 (0.20)	14.31
L7	2.31 (0.50)	2.98 (0.50)	2.93 (0.50)	5.91 (0.50)	14.45
L8	2.19 (0.91)	3.15 (0.32)	2.93 (0.02)	6.11 (0.47)	14.58
L9	2.33 (0.50)	3.18 (0.50)	2.86 (0.50)	6.04 (0.50)	14.72
T0	2.43 (0.50)	2.88 (0.50)	2.88 (0.50)	5.76 (0.50)	14.86
T1	1.47 (0.50)	3.39 (0.50)	3.20 (0.50)	6.59 (0.50)	14.99
T2	1.80 (0.50)	4.25 (0.50)	3.13 (0.50)	7.38 (0.50)	15.13
T3	1.16 (0.33)	3.48 (0.56)	3.27 (0.31)	6.75 (0.87)	15.27
T4	1.04 (0.52)	3.82 (2.02)	3.53 (0.06)	7.35 (2.09)	15.40
T5	***	***	***	***	15.54
T6	1.96 (0.96)	4.00 (0.33)	3.49 (0.06)	7.49 (0.33)	15.68

Note. — The mean and (σ) of each color are given. If there is only one measurement, σ is set equal to (0.50). The J-band absolute magnitudes come from the calibrated spectroscopic parallax relation described in section 5.3 and given in equation 2.

Table 5. SDSS M9, L and T dwarfs with new optical spectra

Name	RA J2000	Dec J2000	r^*	i^*	z^*	J	H	K ¹²	Spectral Type	Source
SDSSJ0022-0110	00:22:09.31	-01:10:40.2	22.69	19.77	17.88	15.83	15.10	14.63	M9	EDR
SDSSJ0223+0006	02:23:57.93	+00:06:22.4	23.16*	20.49	18.72	16.56	16.01	15.57	M9	EDR
SDSSJ0227+0026	02:27:54.92	+00:26:20.0	23.73*:	20.55	18.81	*****	*****	*****	M9	EDR
SDSSJ0228+0040	02:28:15.65	+00:40:26.6	23.42*	20.84	19.30	*****	*****	*****	M9	EDR
SDSSJ0230-0012	02:30:44.46	-00:12:59.3	24.27*:	20.64	19.18	16.99	16.44	15.19	M9	EDR
SDSSJ0233-0023	02:33:11.06	-00:23:30.7	22.72	20.26	18.84	*****	*****	*****	M9	EDR ¹¹
SDSSJ0249-0034	02:49:58.36	-00:34:10.0	22.16	19.38	17.64	15.46	14.80	14.28	M9	EDR
SDSSJ0309-0753	03:09:53.46	-07:53:15.3	23.36*	21.20:	18.60	16.50	15.68	15.40	M9	APO
SDSSJ0443+0002	04:43:37.60	+00:02:05.2	19.74	16.93	15.03	12.52	11.80	11.17	M9	APO
SDSSJ1050+0058	10:50:12.49	+00:58:03.3	23.71*:	20.47	18.57	*****	*****	*****	M9	EDR
SDSSJ1134+0022	11:34:54.89	+00:22:54.5	19.57	16.82	15.05	*****	*****	*****	M9	APO
SDSSJ1342-0027	13:42:28.41	-00:27:05.7	22.26	19.76	17.93	15.59	14.92	14.32	M9	EDR
SDSSJ1413+0016	14:13:21.49	+00:16:37.3	23.33*	20.15	18.53	*****	*****	*****	M9	EDR
SDSSJ1413+5154	14:13:33.87	+51:54:17.2	22.85	19.78	17.94	*****	*****	*****	M9	APO ⁸
SDSSJ1440+0051	14:40:50.61	+00:51:52.3	23.21*:	20.08	18.45	*****	*****	*****	M9	EDR
SDSSJ1635+0008	16:35:21.33	+00:08:24.3	22.56	19.87	18.10	*****	*****	*****	M9	APO ⁸
SDSSJ1648-0012	16:48:21.07	-00:12:27.1	20.54	17.67	15.85	*****	*****	*****	M9	APO ⁸
SDSSJ1707+6439	17:07:18.32	+64:39:33.2	19.39	16.59	14.72	12.56	11.83	11.39	M9 (M9) ⁹	APO ⁹
SDSSJ1714+6351	17:14:28.46	+63:51:30.2	23.55*:	20.49	18.88	*****	*****	*****	M9	EDR ¹¹
SDSSJ1716+5537	17:16:12.81	+55:37:54.6	22.82	19.77	17.85	*****	*****	*****	M9	APO
SDSSJ1719+6053	17:19:13.79	+60:53:10.5	22.24	20.01	18.26	*****	*****	*****	M9	EDR
SDSSJ1723+6321	17:23:17.51	+63:21:19.2	22.82	20.09	18.25	*****	*****	*****	M9	EDR
SDSSJ1734+5355	17:34:17.52	+53:55:20.7	22.17	19.25	17.32	15.06	14.34	13.99	M9	APO
SDSSJ1737+5617	17:37:49.86	+56:17:00.1	23.71*:	20.56	18.92	*****	*****	*****	M9	EDR
SDSSJ1742+5611	17:42:16.83	+56:11:08.2	24.60*:	20.46	18.83	*****	*****	*****	M9	EDR
SDSSJ2147+0101	21:47:27.63	+01:01:04.2	21.67	18.88	17.02	*****	*****	*****	M9	APO
SDSSJ2204-0036	22:04:41.97	-00:36:51.4	22.73	19.80	17.91	15.70	15.08	14.37	M9	APO
SDSSJ2230+0111	22:30:42.38	+01:11:50.2	22.72	19.76	17.98	*****	*****	*****	M9	APO
SDSSJ2244-0029	22:44:39.86	-00:29:39.0	22.24	19.60	17.86	15.82	15.03	14.62	M9	APO
SDSSJ0035+1447	00:35:24.44	+14:47:39.8	23.76*:	21.10	19.33	*****	*****	*****	L0	recent ¹¹
SDSSJ0041+1341	00:41:54.54	+13:41:35.5	21.24	18.78	16.92	14.61	13.78	13.39	L0	APO
SDSSJ0227-0055	02:27:23.77	-00:55:18.6	23.27*	20.94	19.37	*****	*****	*****	L0	EDR ¹¹
SDSSJ0256+0110	02:56:01.86	+01:10:47.2	23.56*	20.47	18.69	*****	*****	*****	L0	EDR
SDSSJ0357-0641	03:57:21.11	-06:41:26.0	22.92	20.18	18.26	15.97	15.04	14.60	L0	recent
SDSSJ0747+3947	07:47:56.31	+39:47:32.9	21.81	19.22	17.42	15.12	14.19	13.71	L0	APO
SDSSJ0752+4136	07:52:59.43	+41:36:34.6	24.08*:	21.03	18.96	16.33	15.66	15.17	L0	recent
SDSSJ1113-0002	11:13:16.95	-00:02:46.6	21.91	19.43	17.50	15.08	14.29	13.77	L0	EDR
SDSSJ1138+6740	11:38:33.10	+67:40:40.3	21.82	19.35	17.52	15.20	14.50	13.95	L0	recent
SDSSJ1148+0254	11:48:04.26	+02:54:05.7	22.59	20.34	18.52	*****	*****	*****	L0	recent
SDSSJ1159+0057	11:59:38.50	+00:57:26.9	21.14	18.57	16.72	*****	*****	*****	L0 (L0) ¹⁰	EDR ¹⁰
SDSSJ1228+0050	12:28:55.38	+00:50:44.1	23.09	20.17	18.18	*****	*****	*****	L0	EDR
SDSSJ1430+0013	14:30:55.90	+00:13:52.1	23.03	20.43	18.54	*****	*****	*****	L0 (M8) ⁶	EDR ³
SDSSJ1435-0046	14:35:17.20	-00:46:12.9	22.99	20.41	18.54	*****	*****	*****	L0	APO
SDSSJ1555+0017	15:55:26.15	+00:17:20.6	22.48	19.27	17.39	*****	*****	*****	L0	APO ⁸
SDSSJ1722+6329	17:22:44.32	+63:29:46.8	22.47	19.74	17.86	*****	*****	*****	L0	EDR
SDSSJ0019+0030	00:19:11.65	+00:30:17.8	21.95	19.42	17.52	*****	*****	*****	L1	recent
SDSSJ0038+1343	00:38:43.99	+13:43:39.5	23.34*	20.33	18.46	15.92	15.16	14.72	L1	recent
SDSSJ0042+1459	00:42:21.15	+14:59:23.9	23.62*:	21.05	19.06	16.62	15.86	15.56	L1	APO
SDSSJ0054-0031	00:54:06.55	-00:31:01.8	22.76	20.20	18.20	15.75	14.91	14.38	L1 (L2) ⁶	recent ³
SDSSJ0211+1410	02:11:28.25	+14:10:03.8	23.62*	20.55	18.62	16.09	15.39	14.93	L1	recent
SDSSJ0350-0518	03:50:48.62	-05:18:12.8	23.43*	20.79	18.91	16.31	15.60	15.08	L1	recent
SDSSJ0626+0029	06:26:21.22	+00:29:34.2	22.91	20.43	18.42	*****	*****	*****	L1	AP0 ⁸
SDSSJ0815+4524	08:15:56.74	+45:24:11.8	22.76	20.60	18.54	16.02	15.24	14.81	L1	recent
SDSSJ0927+6027	09:27:57.46	+60:27:46.3	22.69	19.91	18.07	*****	*****	*****	L1	recent
SDSSJ1045-0149	10:45:23.98	-01:49:57.7	20.05	17.58	15.77	13.13	12.37	11.81	L1	APO
SDSSJ1048+0111	10:48:42.84	+01:11:58.5	19.77	17.23	15.42	*****	*****	*****	L1	recent
SDSSJ1148+0203	11:48:05.02	+02:03:50.9	22.27	19.90	17.90	*****	*****	*****	L1	recent
SDSSJ1402+0148	14:02:31.75	+01:48:30.3	22.33	19.93	17.97	*****	*****	*****	L1	recent
SDSSJ1404+0235	14:04:41.68	+02:35:50.1	22.98	20.00	18.08	*****	*****	*****	L1	recent
SDSSJ1439+0317	14:39:33.44	+03:17:59.2	23.29*	20.66	18.71	*****	*****	*****	L1	recent
SDSSJ1502+6138	15:02:40.80	+61:38:15.5	23.28*	20.68	18.79	16.37	16.07	15.36	L1	recent
SDSSJ1630+0051	16:30:50.01	+00:51:01.3	22.86	20.55	18.81	*****	*****	*****	L1	recent ⁸
SDSSJ1728+5845	17:28:22.19	+58:45:09.9	23.24	21.04	19.05	*****	*****	*****	L1	recent
SDSSJ0235-0849	02:35:47.56	-08:49:19.8	22.34	19.89	18.01	15.52	14.80	14.20	L2	recent
SDSSJ0800+4658	08:00:48.13	+46:58:25.5	22.45	20.00	18.12	15.48	14.57	14.27	L2	recent

Table 5—Continued

Name	RA J2000	Dec J2000	r^*	i^*	z^*	J	H	K ¹²	Spectral Type	Source
SDSSJ1547+0336	15:47:27.23	+03:36:36.3	23.41*	20.46	18.68	*****	*****	*****	L2	recent
SDSSJ1614+0046	16:14:20.50	+00:46:43.6	23.14	20.89	19.10	*****	*****	*****	L2	recent ⁸
SDSSJ1619+0050	16:19:28.31	+00:50:11.9	21.54	18.99	17.11	*****	*****	*****	L2	recent
SDSSJ2259–0051	22:59:13.88	–00:51:58.2	23.81*	20.68	18.93	16.31	15.37	14.99	L2	APO
SDSSJ0207+1355	02:07:35.60	+13:55:56.3	22.34	19.86	18.07	15.42	14.43	13.79	L3	recent
SDSSJ0328+0032	03:28:17.38	+00:32:57.2	22.90	20.61	18.88	*****	*****	*****	L3 (L2.5) ⁶	recent ³
SDSSJ1435–0043	14:35:35.72	–00:43:47.0	24.30*	20.90	19.02	*****	*****	*****	L3	APO
SDSSJ1440+0026	14:40:16.20	+00:26:38.9	22.94	20.71	18.77	*****	*****	*****	L3	recent
SDSSJ1653+6231	16:53:29.69	+62:31:36.5	21.54	19.51	17.61	*****	*****	*****	L3	EDR
SDSSJ2028+0052	20:28:20.32	+00:52:26.5	21.37	18.89	17.04	*****	*****	*****	L3	APO ⁸
SDSSJ2140+0112	21:40:46.55	+01:12:59.7	23.38*	21.10	18.96	*****	*****	*****	L3	APO
SDSSJ2249+0044	22:49:53.46	+00:44:04.6	23.98*	22.03	19.44	16.46 ⁷	15.42 ⁷	14.43 ⁷	L3 (L5) ⁵	APO ⁴
SDSSJ0330–0025	03:30:35.12	–00:25:34.6	22.31	20.14	18.04	15.29	14.42	13.83	L4 (L2) ⁶	recent ¹
SDSSJ0805+4812	08:05:31.84	+48:12:33.0	22.72	19.90	17.59	14.71	13.91	13.42	L4	APO
SDSSJ1257–0113	12:57:37.26	–01:13:36.1	22.94	20.78	18.55	15.86	14.70	14.13	L4 (L5) ⁵	recent ⁴
SDSSJ1717+6526	17:17:14.10	+65:26:22.2	22.54	20.21	17.77	14.94	13.85	13.20	L4	APO
SDSSJ0127+1354	01:27:43.51	+13:54:20.9	23.57*	22.08	19.61	*****	*****	*****	L5	APO
SDSSJ0801+4628	08:01:40.53	+46:28:49.5	23.36*	21.28	18.80	16.29	15.44	14.54	L5 (L6.5) ¹³	APO ¹³
SDSSJ0236+0048	02:36:17.94	+00:48:54.8	25.04*	21.50	18.92	16.01 ⁷	15.16 ⁷	14.54 ⁷	L6 (L6.5) ⁵ (L6) ⁶	EDR ³
SDSSJ1331–0116	13:31:48.92	–01:16:51.4	22.78	20.59	18.16	15.46	14.44	14.08	L6	APO
SDSSJ1446+0024	14:46:00.60	+00:24:52.0	23.39*	20.74	18.54	15.56 ⁷	14.59 ⁷	13.80 ⁷	L6 (L5) ⁵	APO ⁴
SDSSJ0857+5708	08:57:58.45	+57:08:51.4	23.02	20.71	17.73	14.80 ⁷	13.80 ⁷	12.94 ⁷	L7 (L8) ⁵	APO ⁴
SDSSJ0107+0041	01:07:52.34	+00:41:56.1	24.06*	21.52	18.66	15.75 ⁷	14.56 ⁷	13.58 ⁷	L8 (L5.5) ⁵ (L7) ⁶	EDR ³
SDSSJ1207+0244	12:07:47.17	+02:44:24.8	24.37*	21.49	18.40	*****	*****	*****	L8	recent
SDSSJ0830+4828	08:30:08.12	+48:28:47.5	23.59*	21.26	18.08	15.22 ⁷	14.40 ⁷	13.68 ⁷	L9 ⁵	recent ⁴
SDSSJ0423–0414	04:23:48.56	–04:14:03.5	22.64	20.21	17.33	14.45	13.44	12.94	TO ⁵ (L5) ⁶	APO ^{3,8}
SDSSJ0151+1244	01:51:41.68	+12:44:29.6	24.31*	22.84*	19.45	16.25 ⁷	15.54 ⁷	15.18 ⁷	T1 ⁵	APO ⁴
SDSSJ1254–0122	12:54:53.90	–01:22:47.4	24.06*	22.26*	18.01	14.88	14.04	13.83	T2 ⁵	recent ²
SDSSJ1021–0304	10:21:09.69	–03:04:20.1	23.31*	22.39*	19.31	16.26	15.33	15.10	T3 ⁵	APO ²

Note. — Comments:

* — Magnitude is fainter than formal 5σ limits: $r^* = 23.1$; $i^* = 22.3$; $z^* = 20.8$

: — Magnitude uncertainty is greater than $r^* = 0.5$; $i^* = 0.2$; $z^* = 0.2$

1 — First identified by Fan et al. (2000)

2 — First identified by Leggett et al. (2000)

3 — First identified by Schneider et al. (2002)

4 — First identified by Geballe et al. (2002)

5 — Spectral type given by Geballe et al. (2002)

6 — Spectral type given by Schneider et al. (2002)

7 — near-IR observations reported by Leggett et al. (2002), in the MKO filter system

8 — Photometry from preliminary processing of data not contained in the final SDSS database

9 — Identified by, and spectral type from, Gizis et al. (2000) as 2MASSW J1707+6439

10 — Identified by, and spectral type from, Martin et al. (1999) as DENISp 1159.6+0057

11 — Position within released 2MASS survey limits; object not detected in IR

12 — The K band data are from 2MASS unless otherwise noted, and were obtained in the 2MASS K_s filter

13 — Identified by, and spectral type from, Kirkpatrick et al. (2000) as 2MASSW J0801+4628

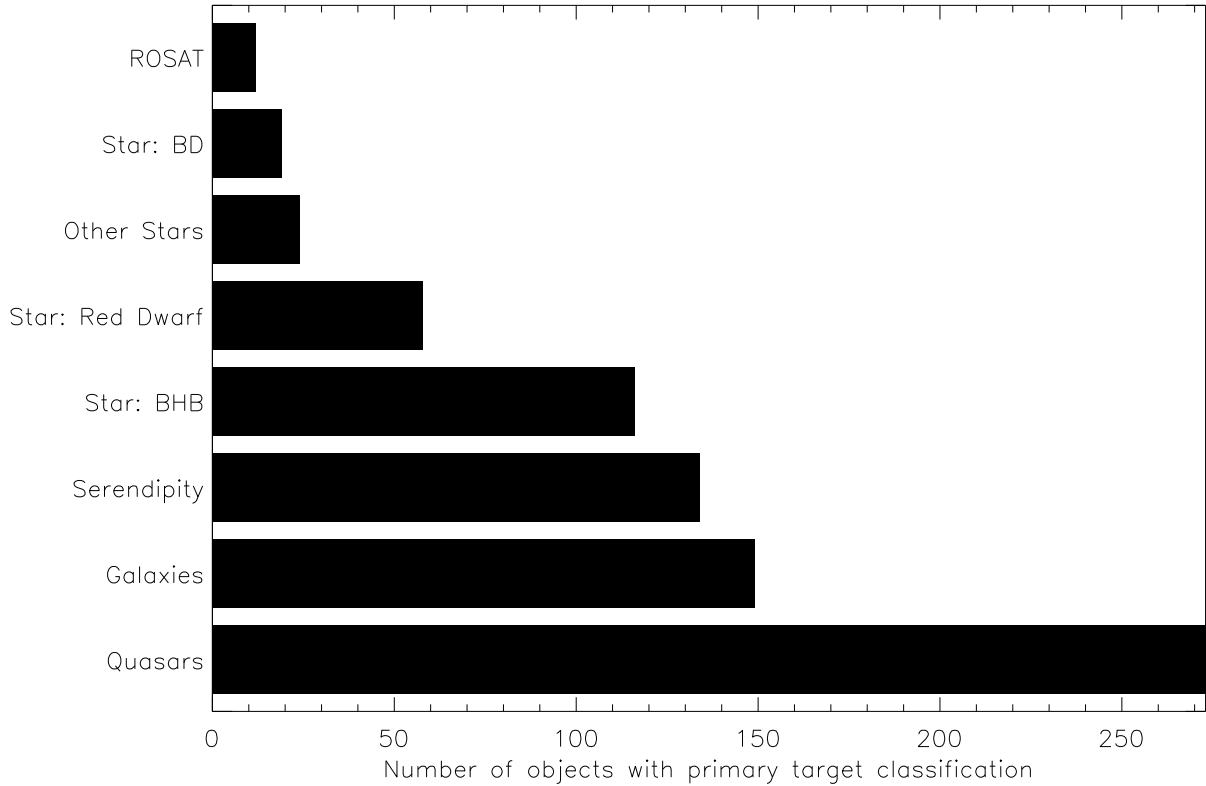


Fig. 1.— SDSS primary targetting assignments are shown for objects that subsequently turned out to be M and L dwarfs in the SDSS EDR spectra. Most of the objects were originally targetted as quasars and galaxies, or by the serendipity category which targets objects with unusual colors. The Star: BD label refers to brown dwarfs. As described in the text, the large number of objects in the Star: BHB (blue horizontal branch) category is the result of a single plate to check objects with stellar colors.

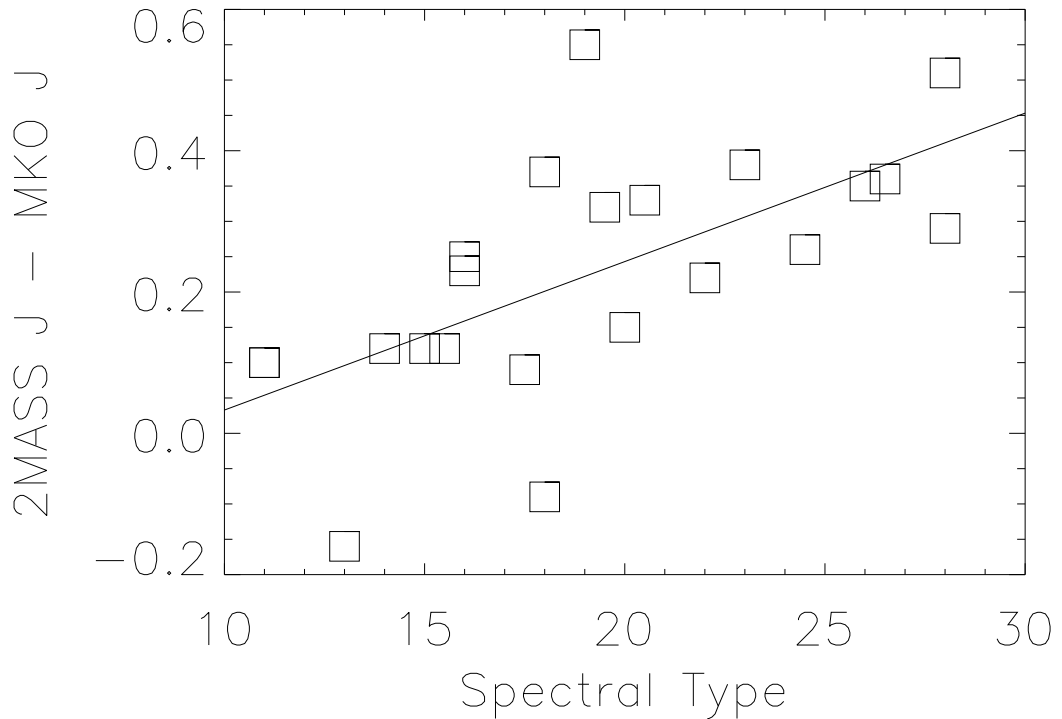


Fig. 2.— The difference between the 2MASS J magnitude and the MKO J magnitude is plotted for 21 late type dwarfs measured with both systems. Numerical spectral types are assigned as M0=0, M5=5, L0=10, L5=15, T0=20, T5=25 here and in all subsequent figures where numerical spectral types are used for fits. The linear least squares fit shown is given in the text. MKO J magnitudes given in Table 5 (and in Leggett et al. (2002) for other previously published objects in the sample), were transformed to the 2MASS system using this relation.

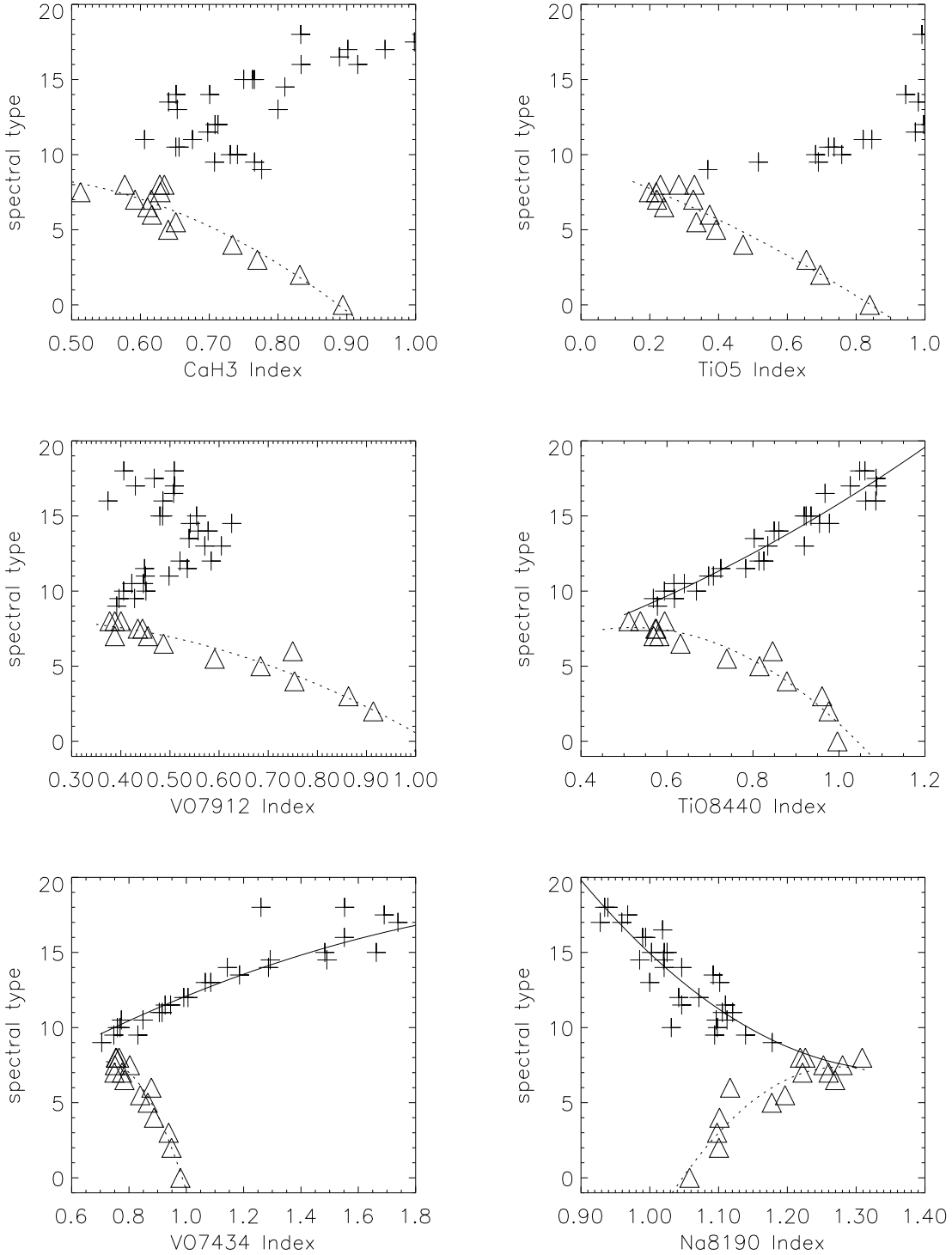


Fig. 3.— Numerical spectral type is plotted vs. the value of the spectral index for six different spectral indices. Open triangles depict M0-M8 dwarfs, while plus signs indicate M9 and later type dwarfs. The lines are second-order polynomial, least squares fits, with the dotted lines applicable for types M0-M8 and the solid lines applicable for types M9-L8. The VO7434 fit applies only through type L6 as described in the text.

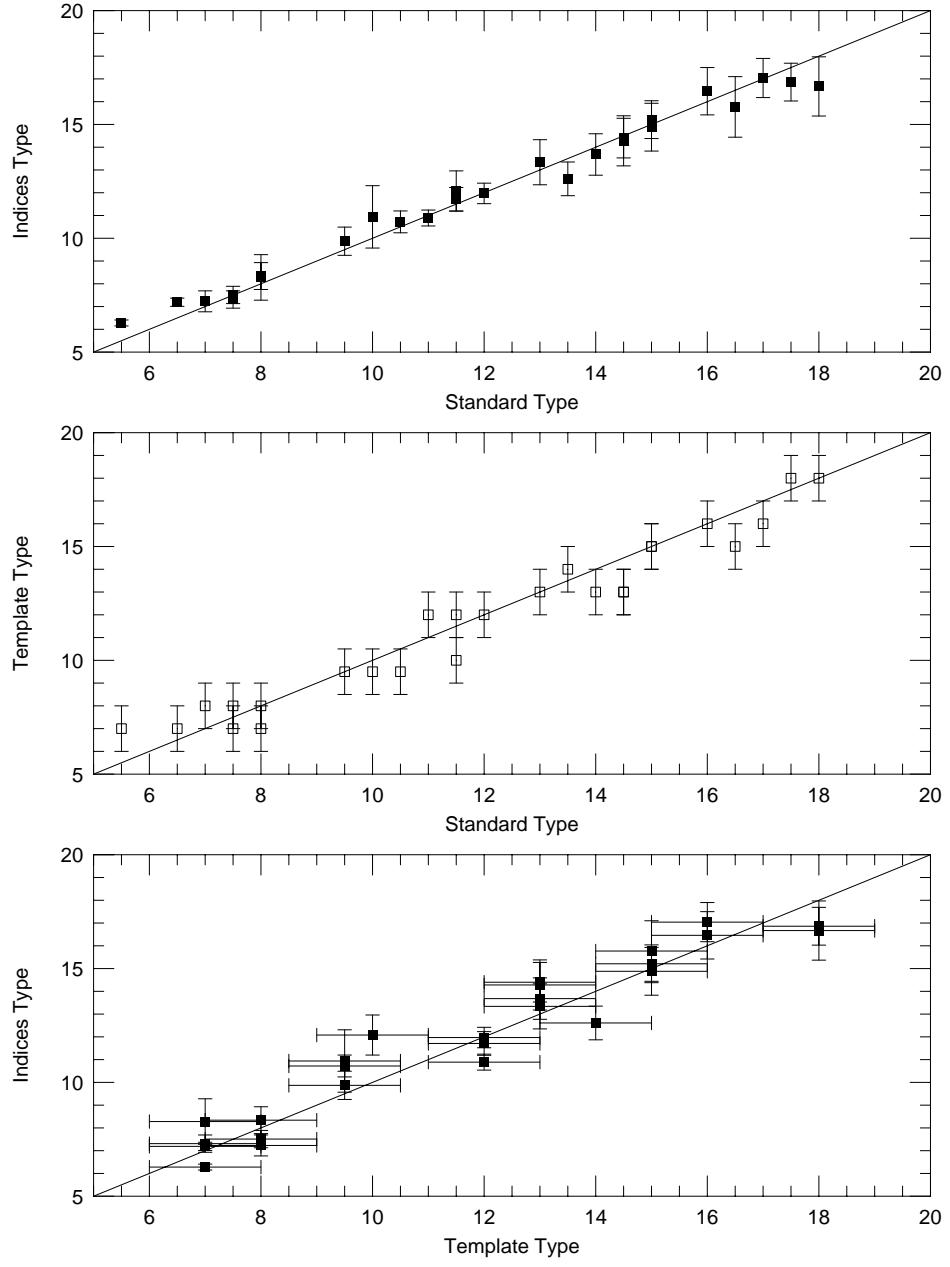


Fig. 4.— The panels show the index and template types compared with the standard types, and compared with each other. Only the additional standards above those given in Table 1 are shown, to avoid matching templates against themselves.

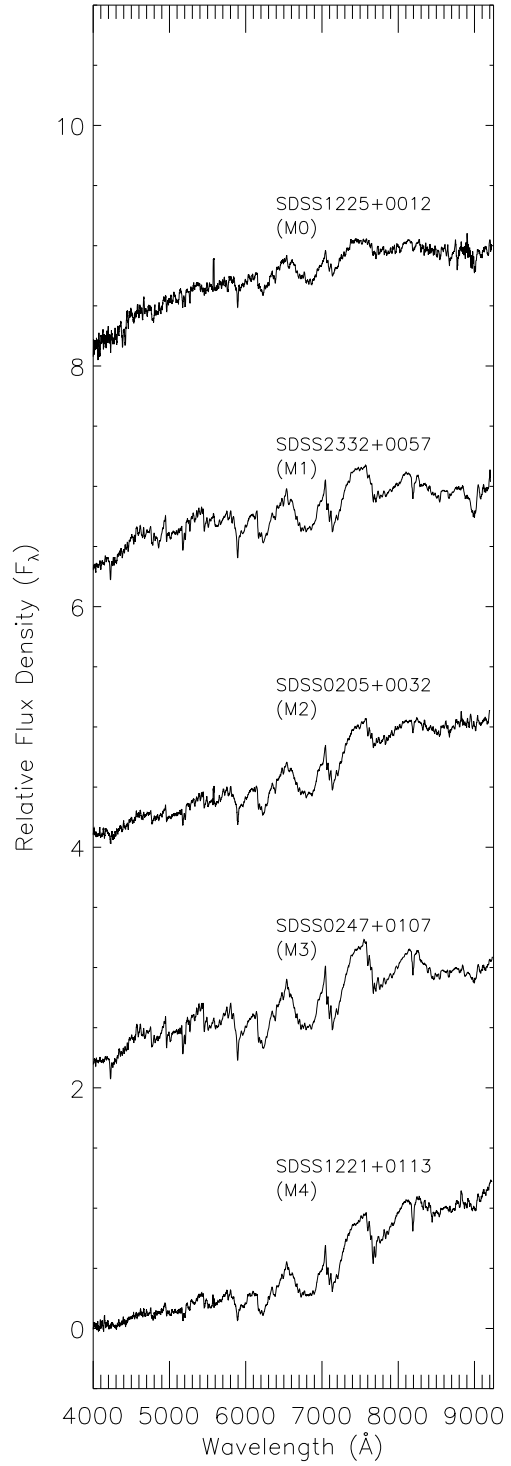


Fig. 5a.— The SDSS spectrum with highest signal-to-noise ratio at each spectral type is shown. These spectra comprise a set of templates to be used in the SDSS pipeline processing for automatic spectral type identification in the future.

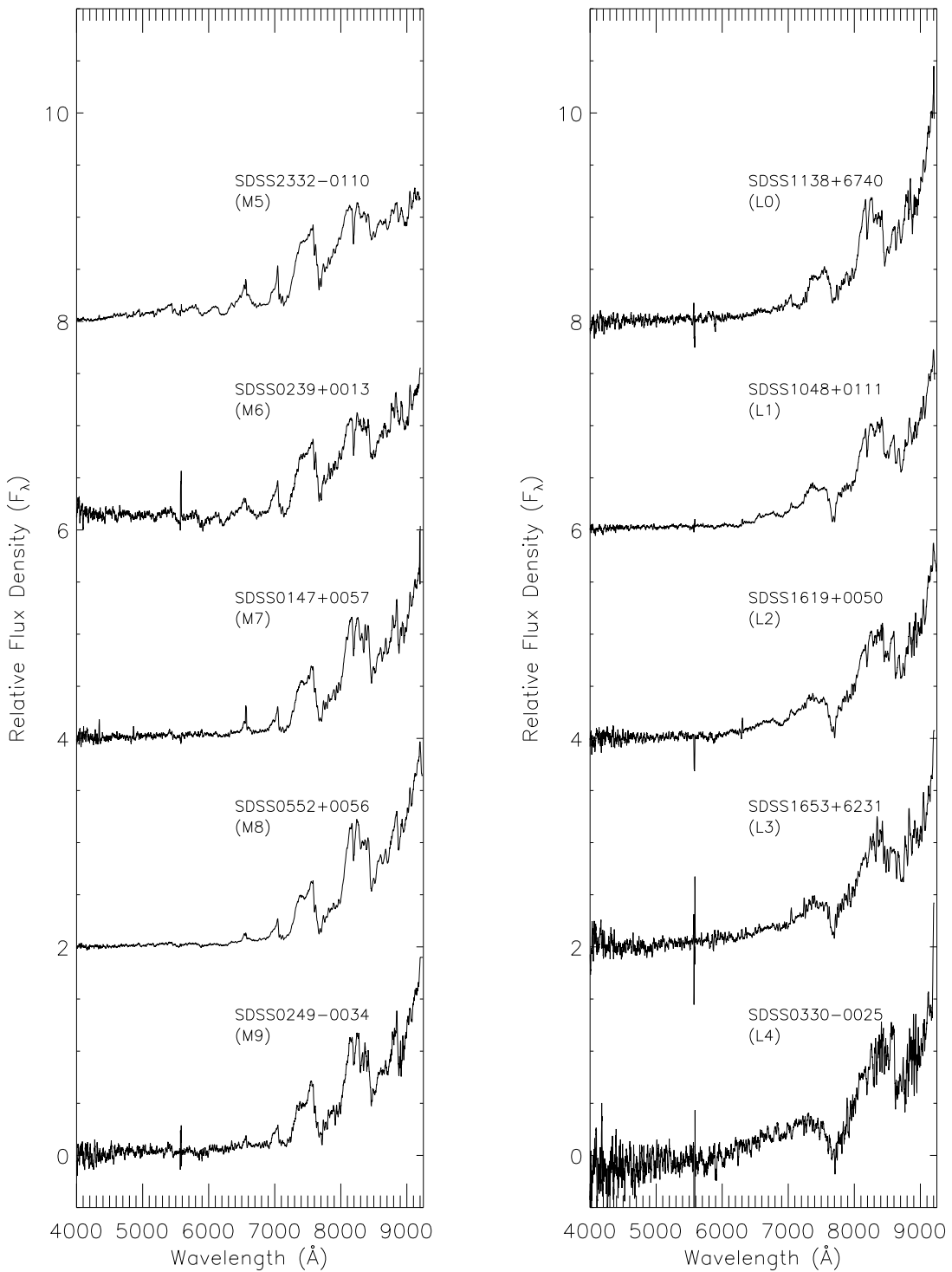


Fig. 5b.— Same as Figure 5a.

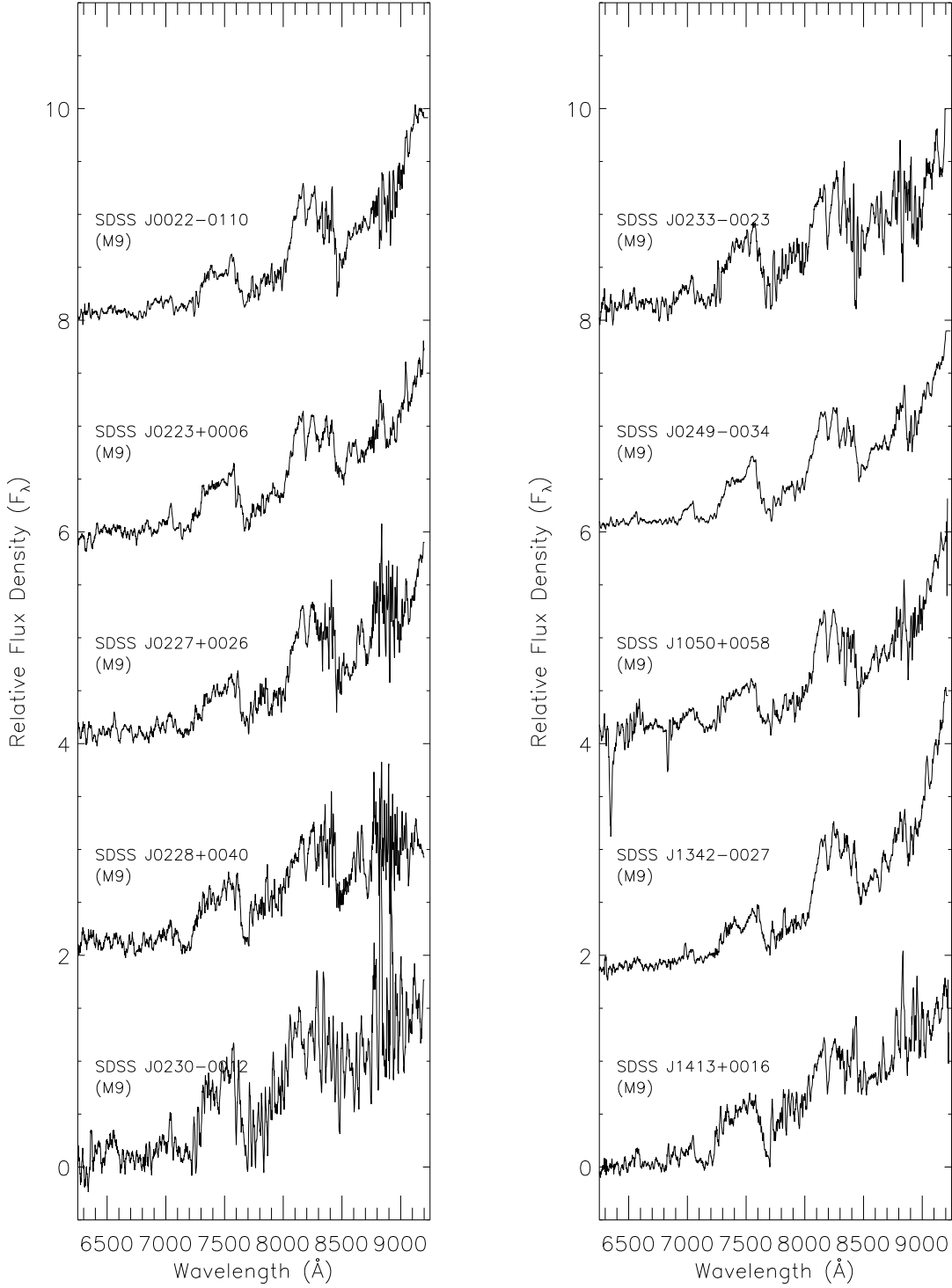


Fig. 6a.— SDSS spectra for all objects M9 and later are shown. The spectral types are ours, as given in Table 5, except for the L9 and T dwarfs where they are taken from previously published sources as described in the table notes.

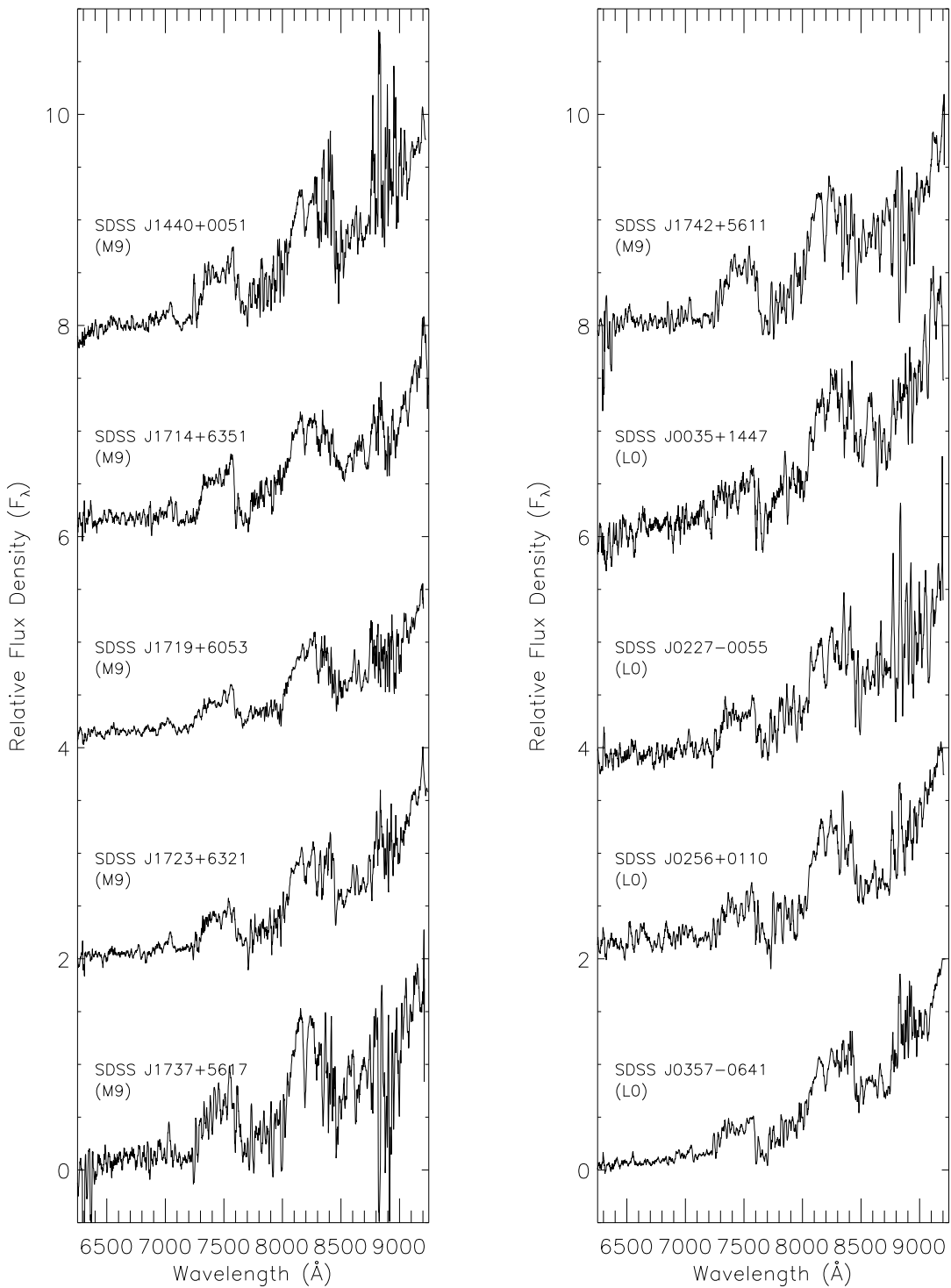


Fig. 6b.— Same as Figure 6a.

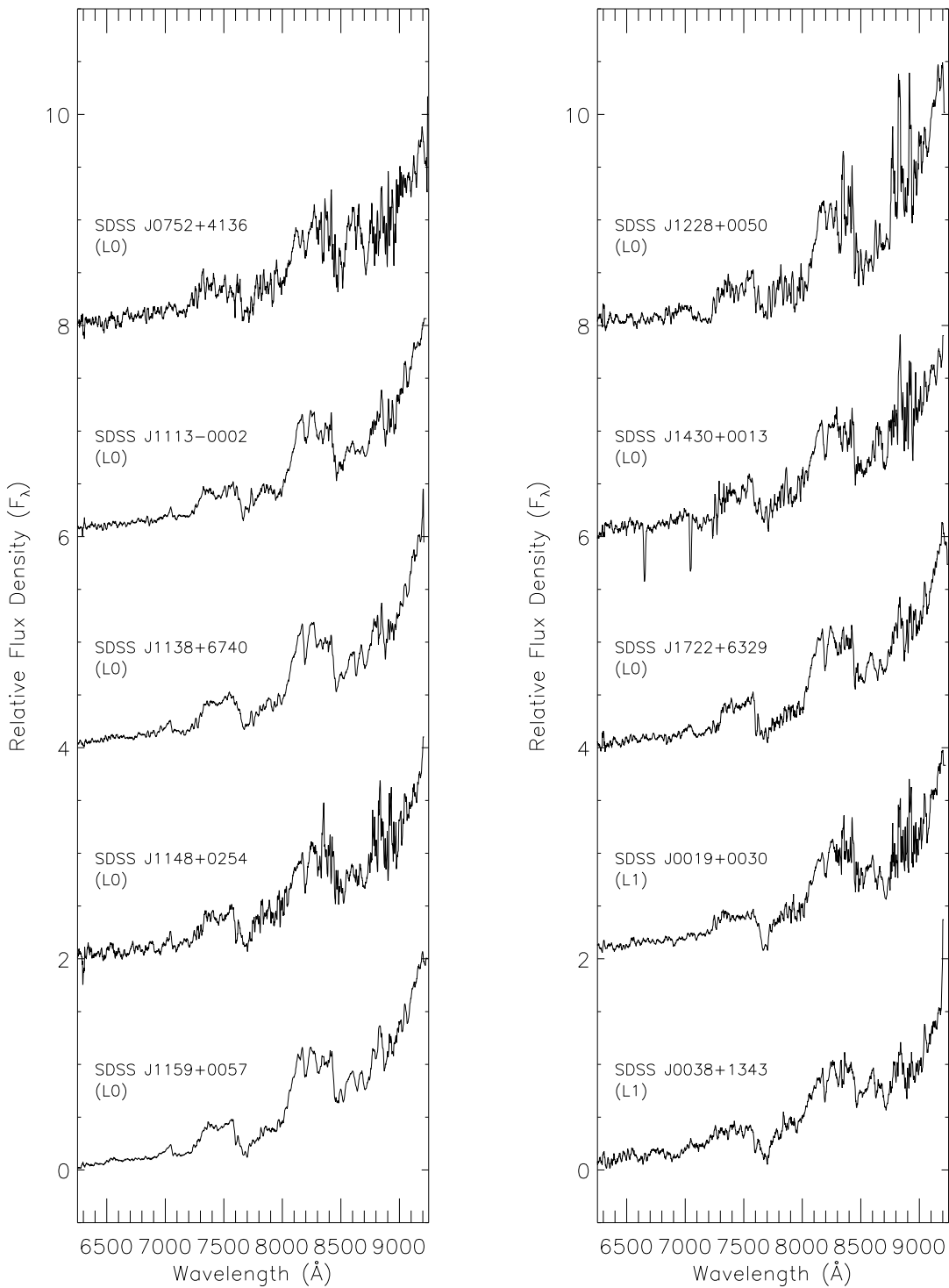


Fig. 6c.— Same as Figure 6a.

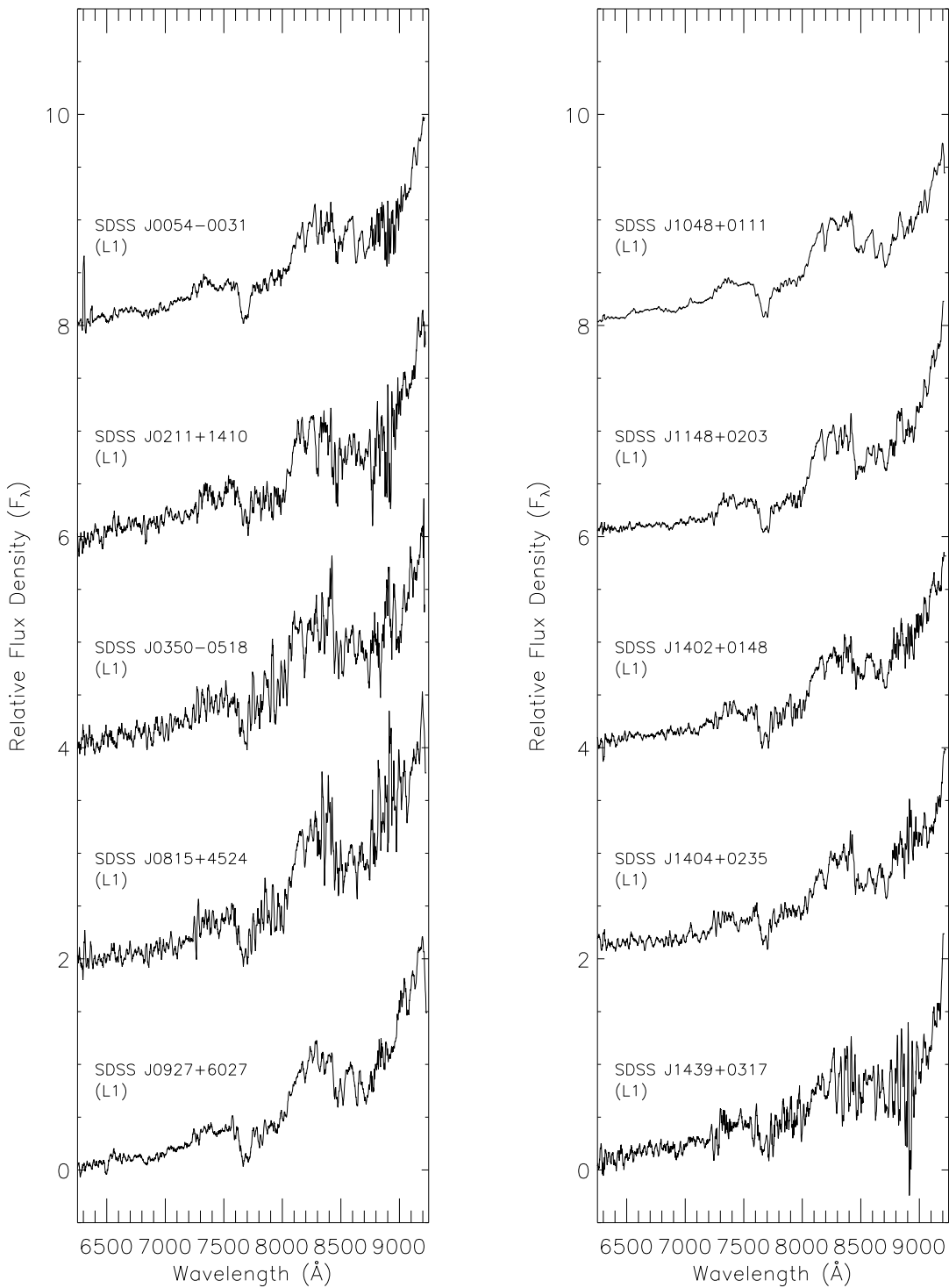


Fig. 6d.— Same as Figure 6a.

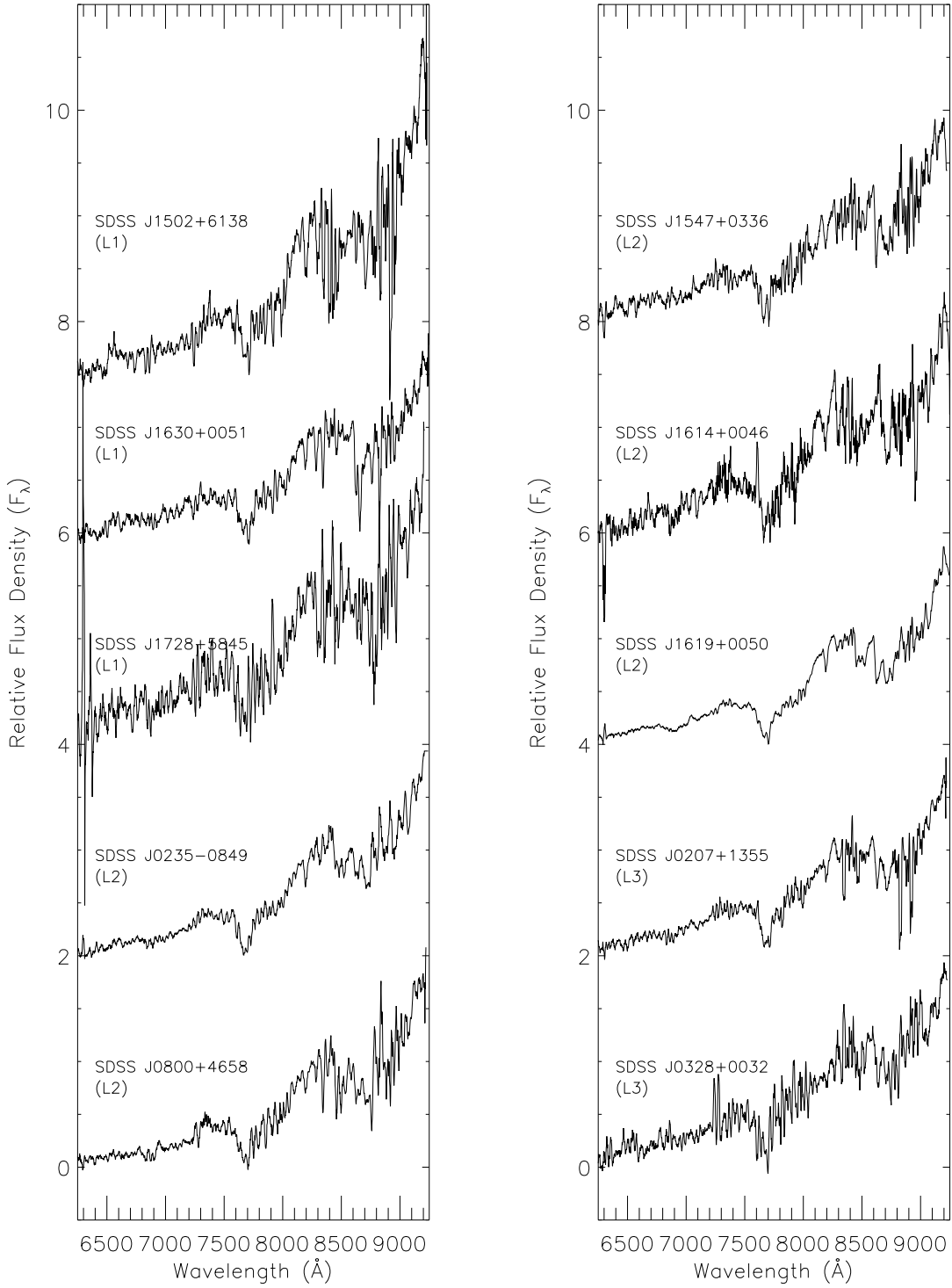


Fig. 6e.— Same as Figure 6a. Note that we have not attempted to remove noise spikes such as those in the left panel near 6300 Å.

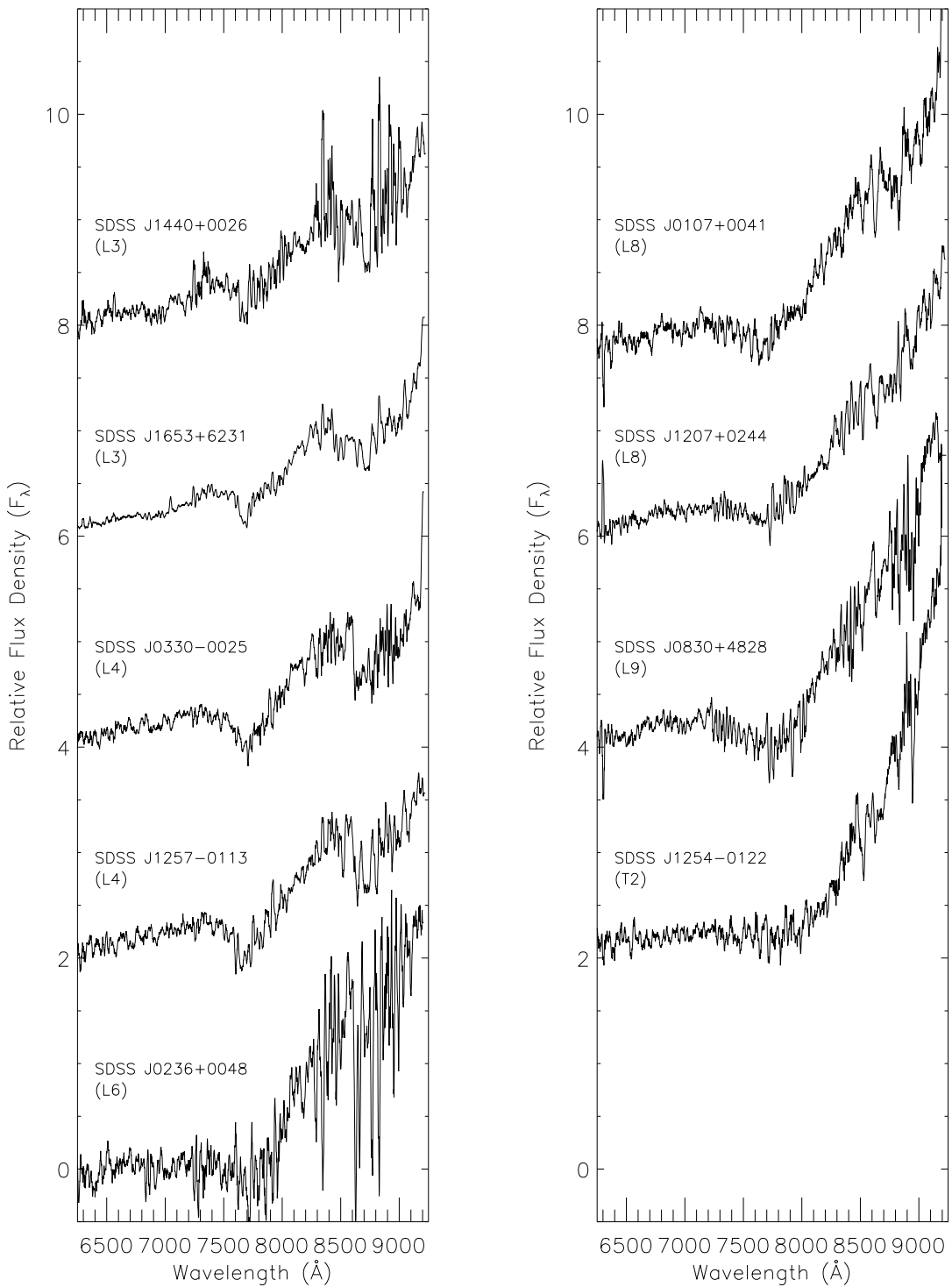


Fig. 6f.— Same as Figure 6a.

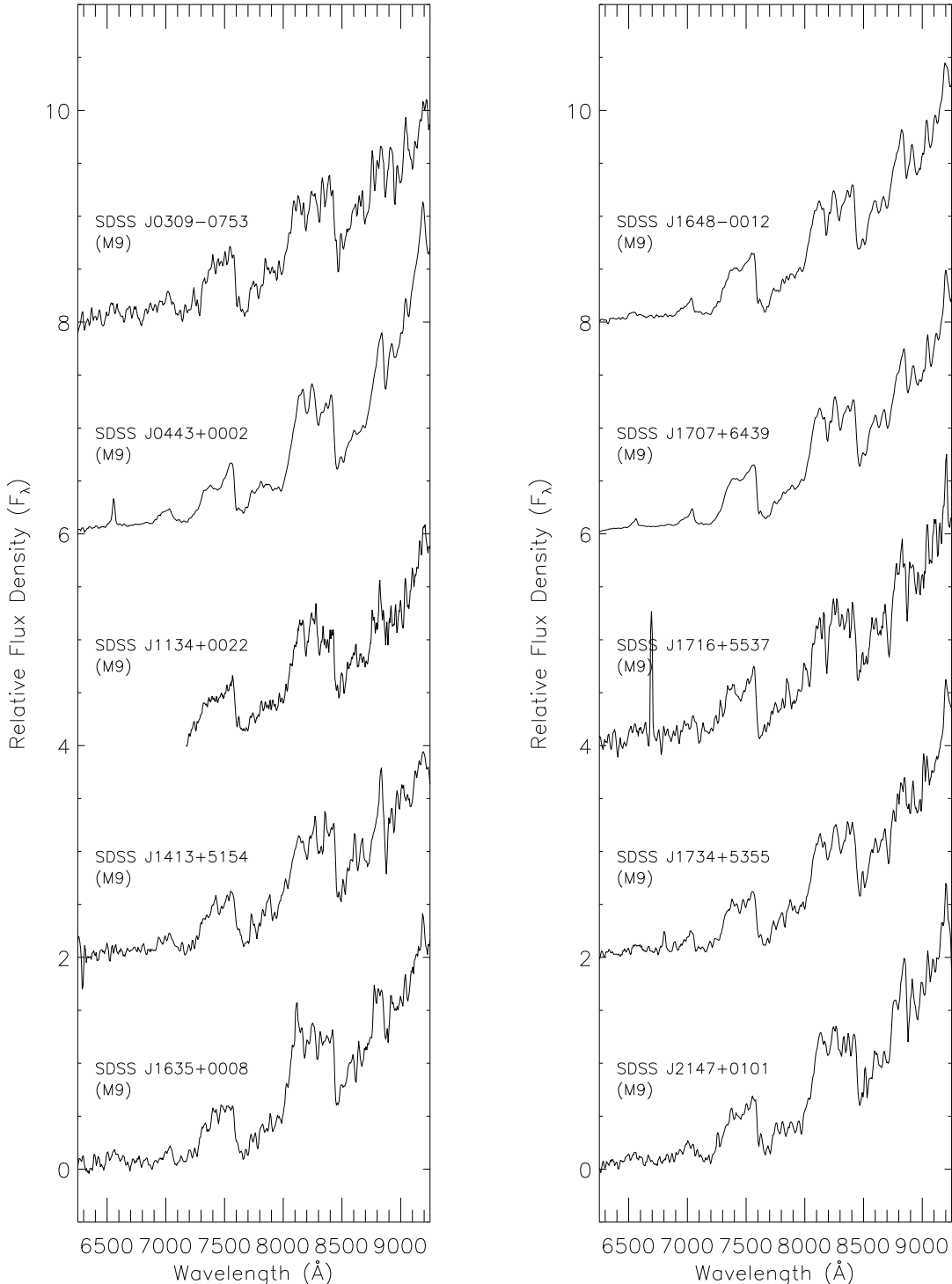


Fig. 7a.— APO 3.5m spectra for all objects M9 and later are shown. The spectral types are ours, as given in Table 5, except for the T dwarfs where they are taken from previously published sources as described in the table notes. These targets were chosen from SDSS imaging data to be very red in the SDSS ($i^* - z^*$) color, producing most of the new mid-late L dwarf spectra in our sample. Note that we have not attempted to remove noise spikes such as the one near 6700Å in SDSSJ1716+5537.

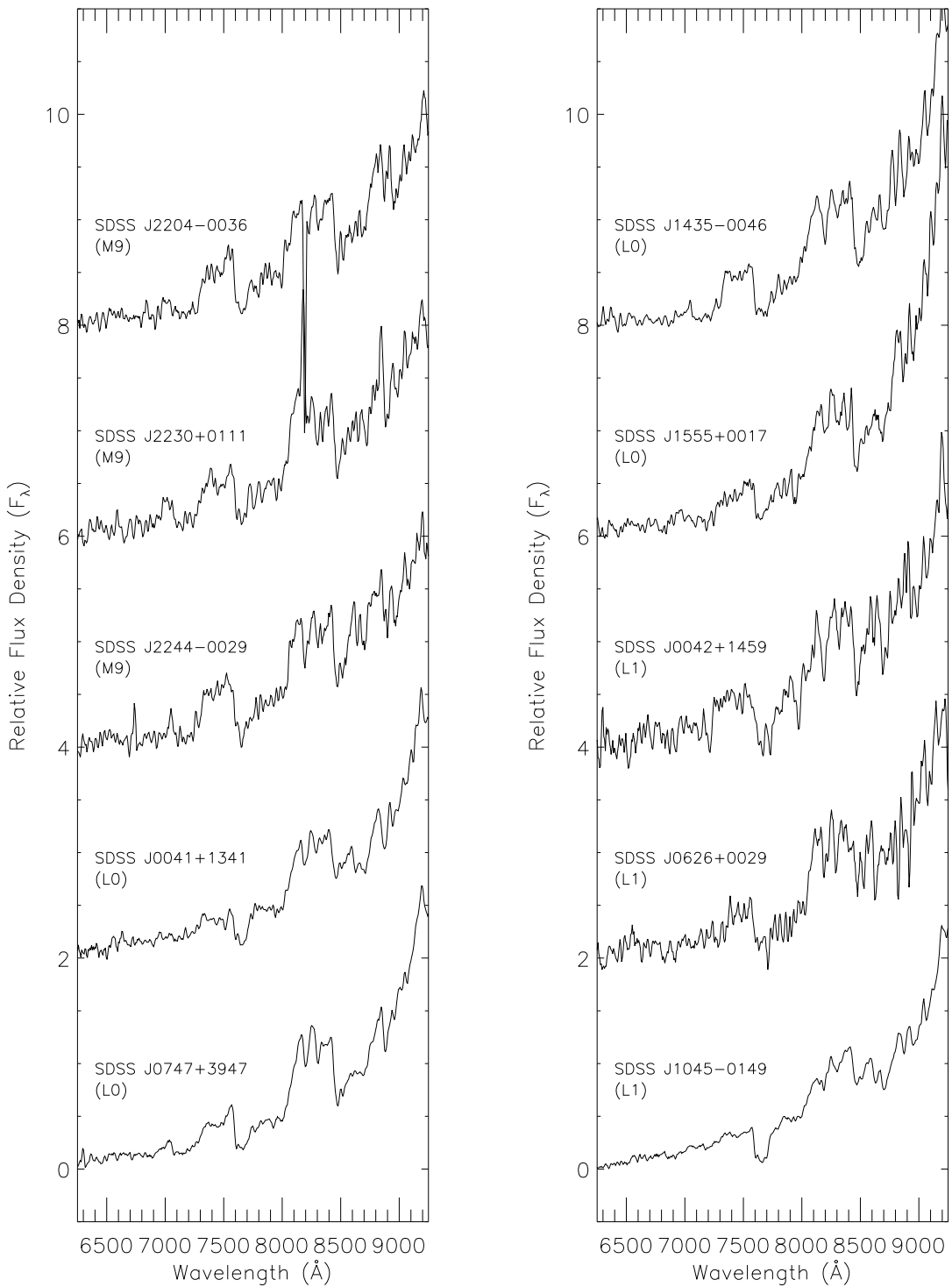


Fig. 7b.— Same as Figure 7a.

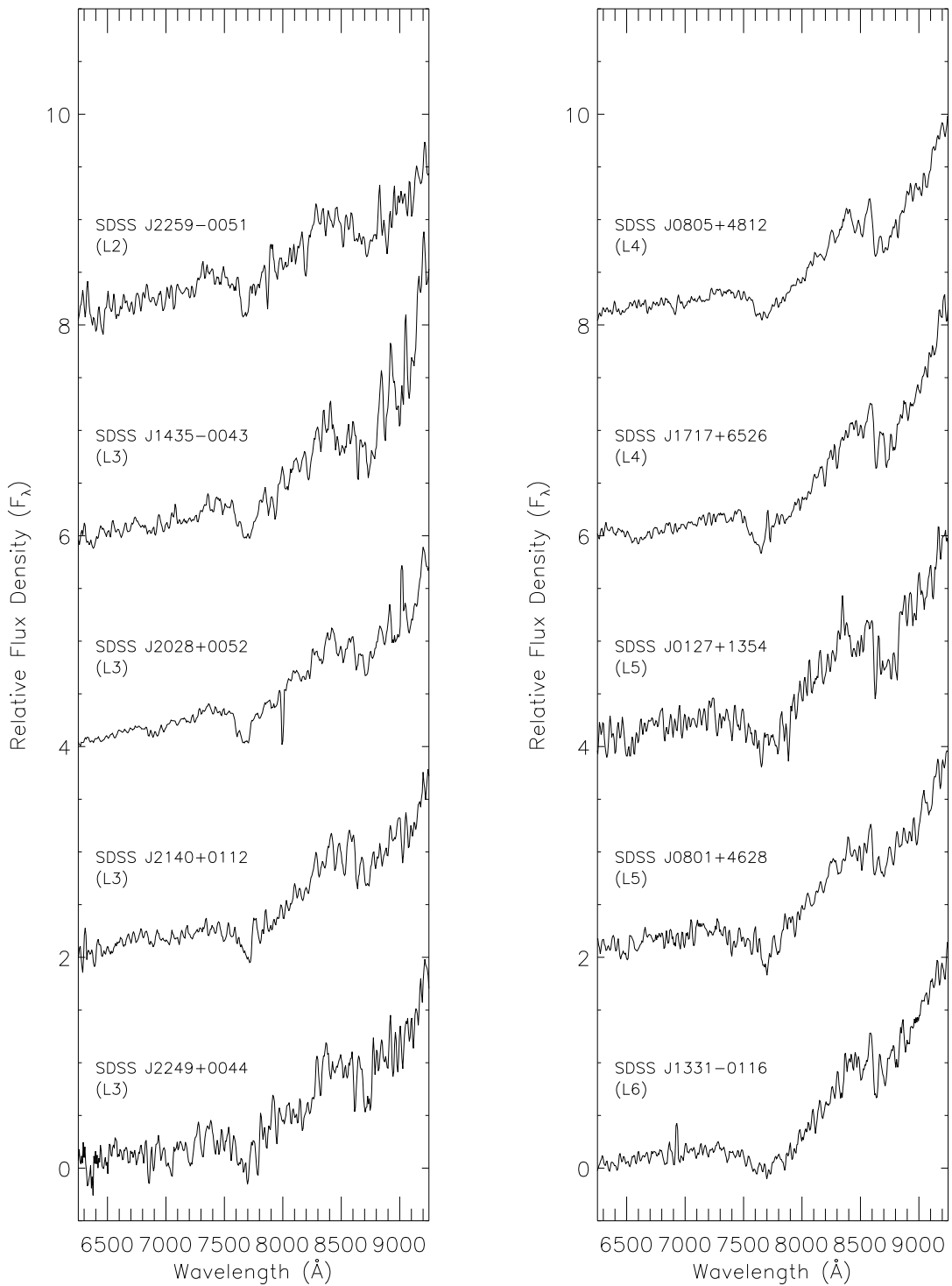


Fig. 7c.— Same as Figure 7a.

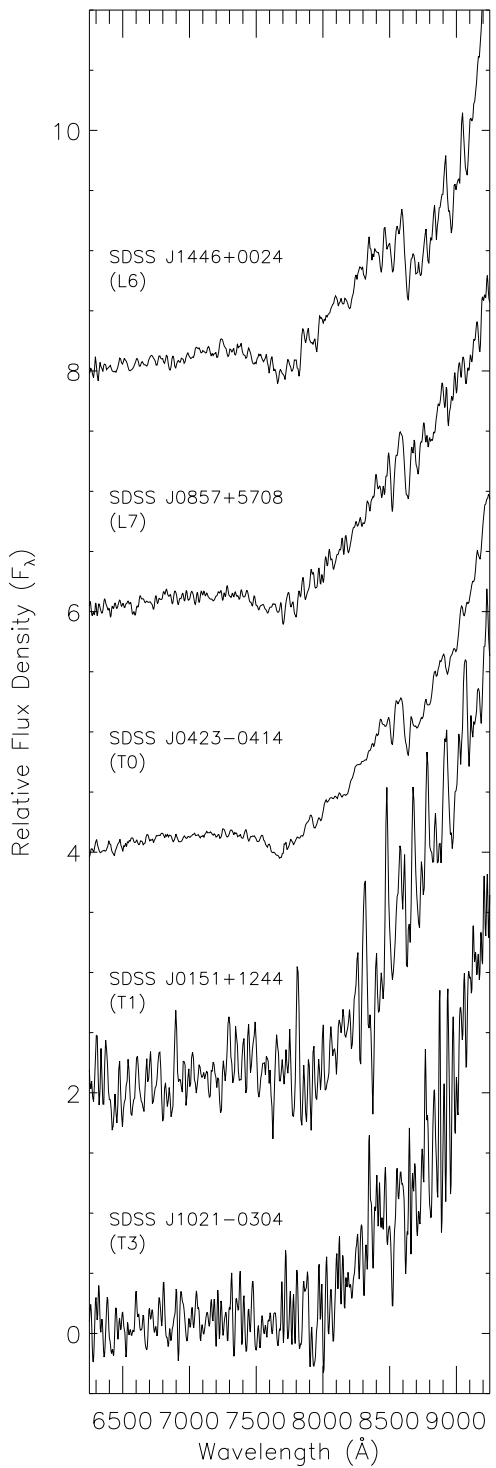


Fig. 7d.— Same as Figure 7a.

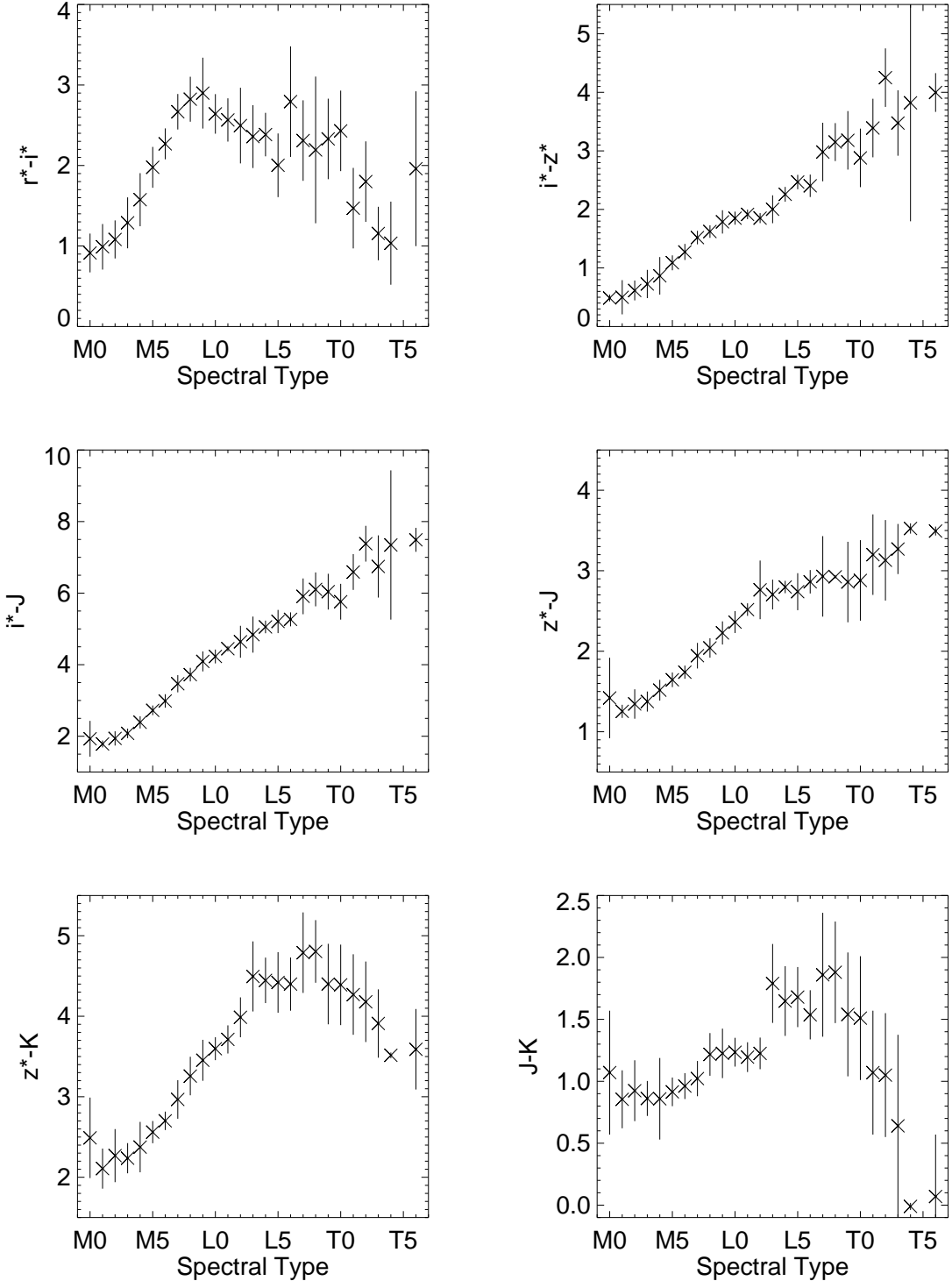


Fig. 8.— Average color – spectral type relations for the full sample are shown. The error bars indicate the standard deviation of the mean color at each spectral type. If only one object of a given type was measured, the standard deviation was set to 0.5.

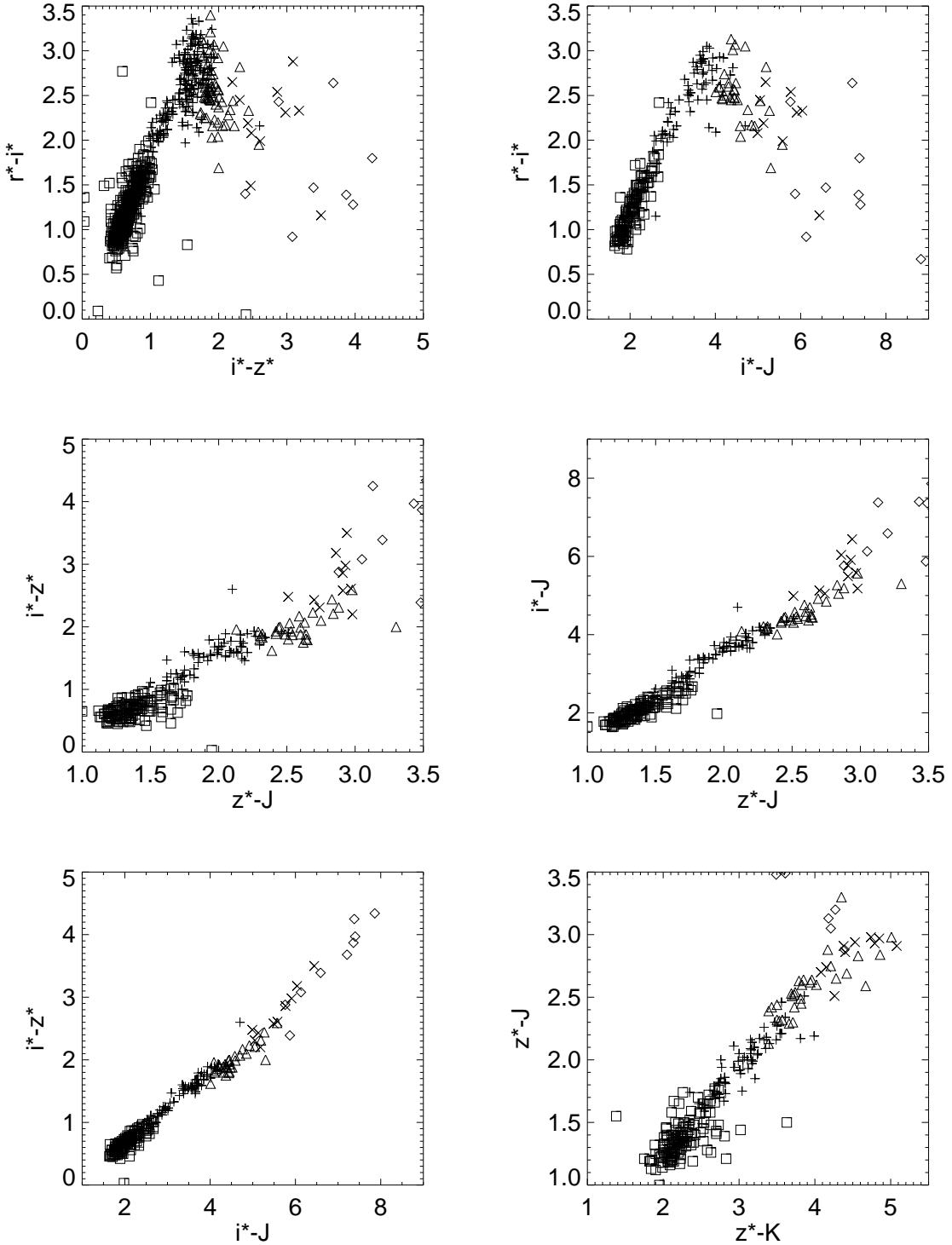


Fig. 9.— Color-color relations for the full sample are shown. Open squares have types M0-M4; plus signs have types M5-M9; open triangles have types L0-L4; crosses have types L5-L9; and open diamonds have types T0-T8.

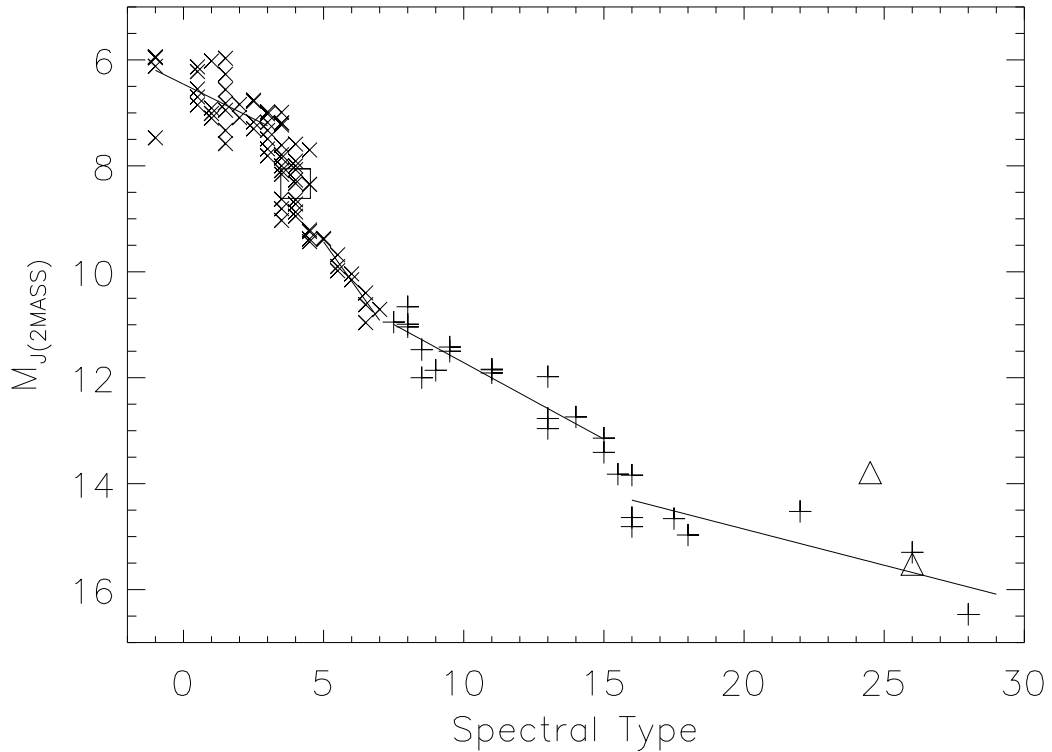


Fig. 10.— Calibrated M_J vs spectral type relation for late type dwarfs with measured 2MASS J magnitudes and distances from trigonometric parallax determinations. Crosses (types M0-M7) come from the 8-pc sample; plus signs (types M8-T8) are from several sources as described in the text. The open triangles are 2MASSJ0559-1404 (T4) and Gl 299B (T6) which are not included in the fit (see text). The solid lines represent our best piecewise linear fit to the data. The large open square at type M4 is our adopted mean value.

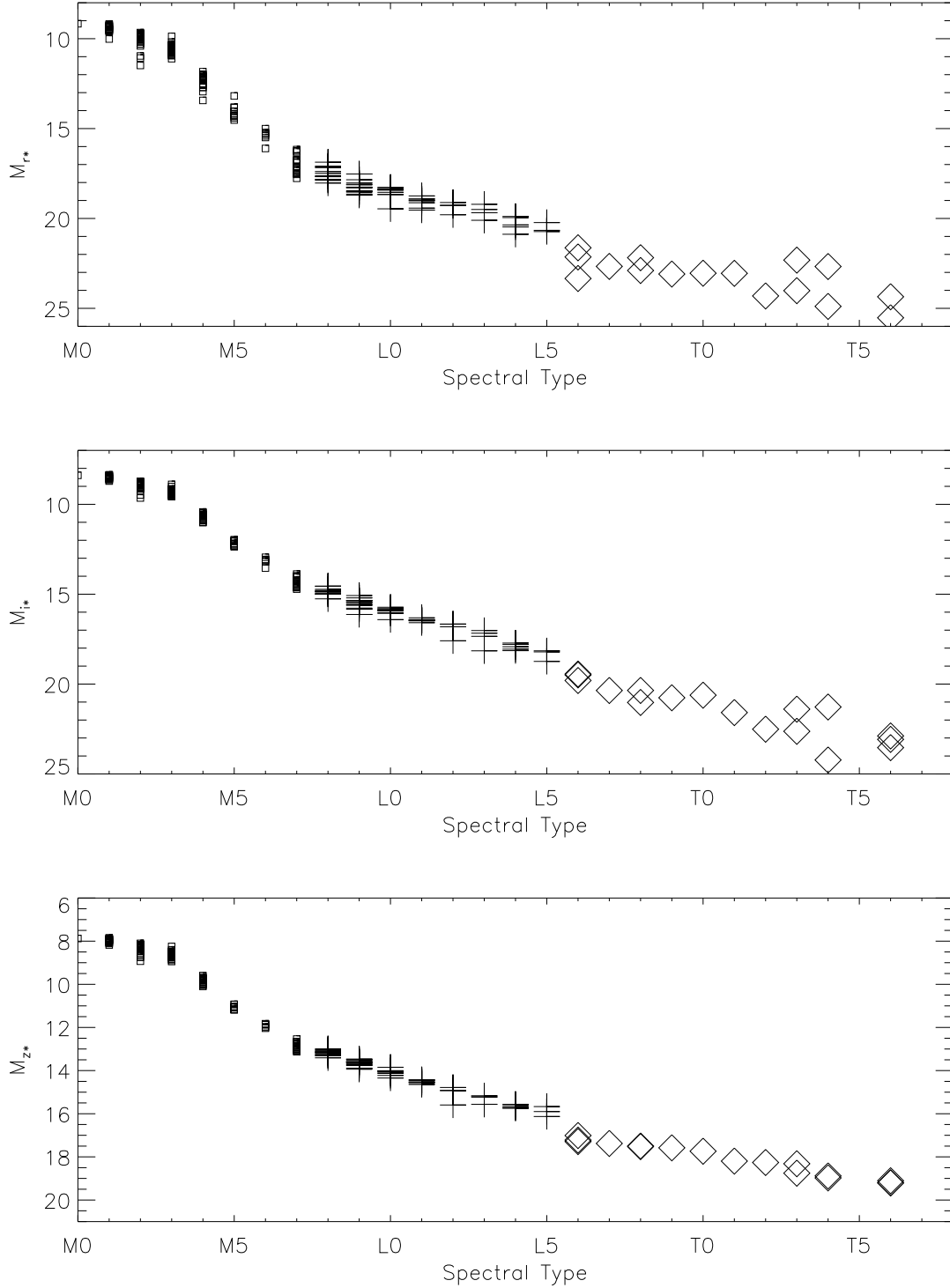


Fig. 11.— Spectroscopic parallax relations for M_{r*} , M_{i*} and M_{z*} , using the fits shown in Figure 10 and our measured colors. Only M dwarfs with 2MASS J magnitudes are shown. L and T dwarfs with MKO J magnitudes were transformed using Equation 1. Small open squares depict types M0-M7, plus signs are used for M8-L5 and open diamonds for L6-T8.

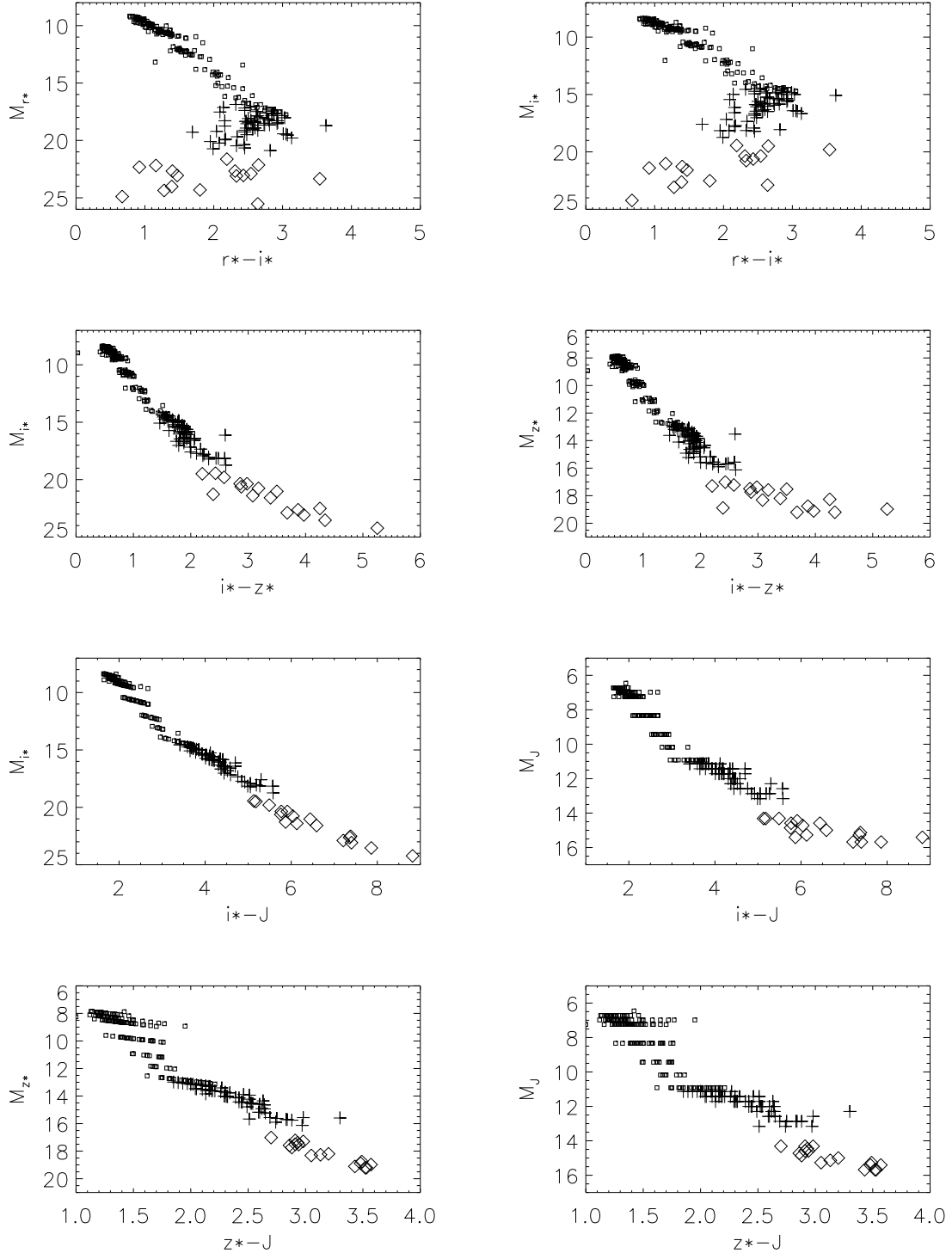


Fig. 12.— Photometric parallax relations for color combinations using the r^* , i^* , z^* and 2MASS J magnitudes. Symbols are the same as in Figure 11.

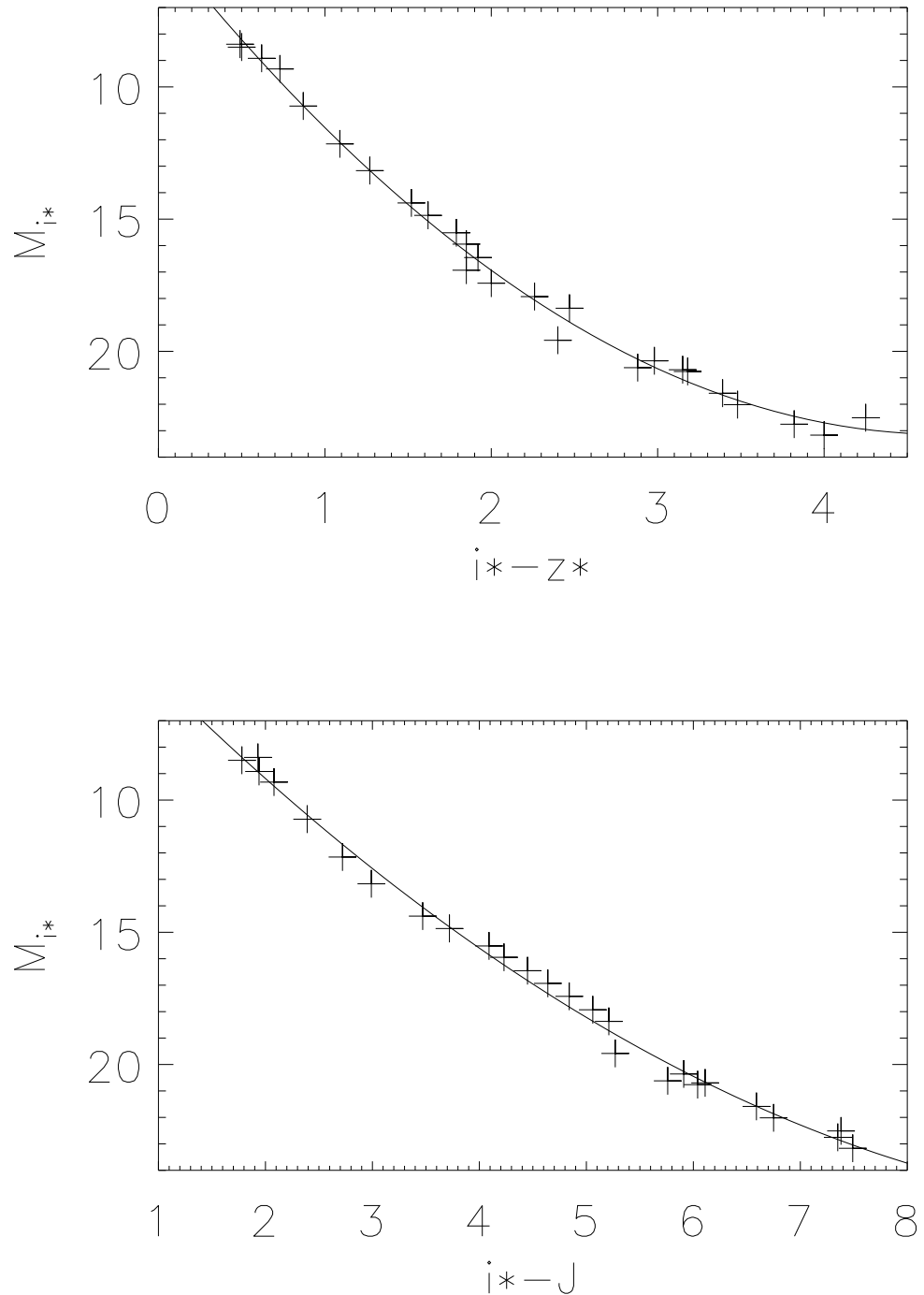


Fig. 13.— Adopted photometric parallax relations for $M_{i^*},(i^* - z^*)$ and $M_{i^*},(i^* - J)$. The best fit second-order polynomial relations are shown by solid lines and given in the text.

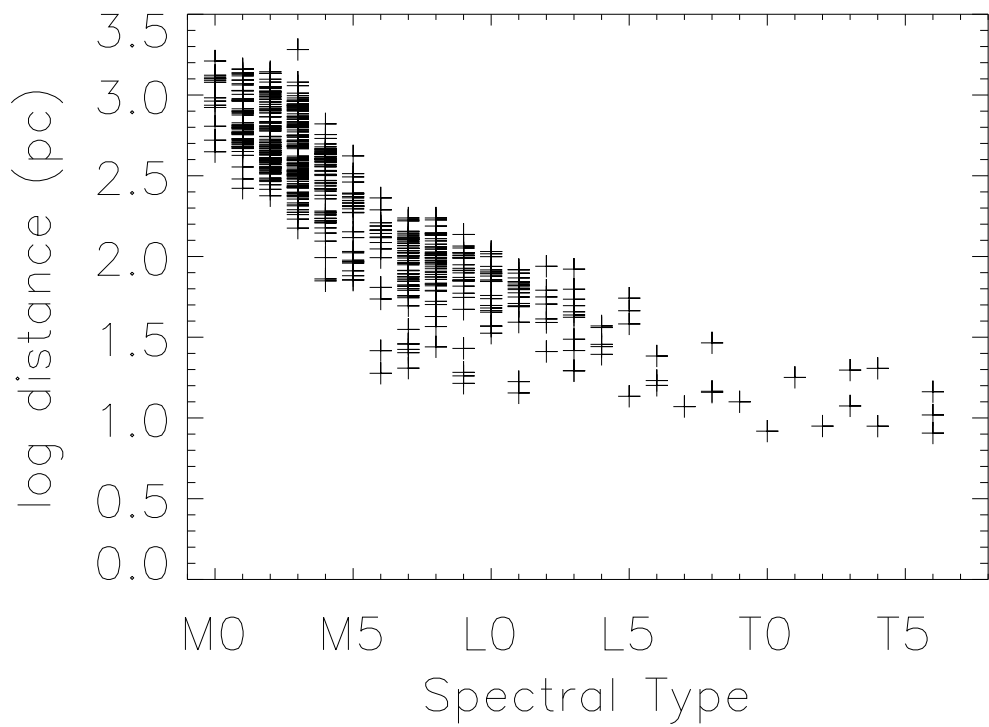


Fig. 14.— Spectroscopic distance estimates for all objects with measured spectral types. The early M dwarfs extend out to ~ 1.5 kpc while the L dwarfs are confined to ~ 100 pc and the T dwarfs to ~ 20 pc.